

BINDING OF THE RESPIRATORY CHAIN INHIBITOR ANTIMYCIN TO THE MITOCHONDRIAL bc_1 COMPLEX: A NEW CRYSTAL STRUCTURE REVEALS AN ALTERED INTRAMOLECULAR HYDROGEN-BONDING PATTERN.

Li-shar Huang, David Cobessi, Eric Y. Tung, and Edward A. Berry

Lawrence Berkeley National Laboratory, Berkeley, CA, USA

**From the Physical Biosciences Division, Lawrence Berkeley National Laboratory
1 Cyclotron Road, Berkeley, California, 94720**

Address correspondence to: Edward A. Berry, Lawrence Berkeley National Lab,
Mailstop 64R243, 1 Cyclotron Road, Berkeley CA 94720, Tel. 510 486-4335;
Fax: 510 588-4829; email: EABerry@LBL.gov

Antimycin A (antimycin), one of the first known and most potent inhibitors of the mitochondrial respiratory chain, binds to the quinone reduction site of the cytochrome bc_1 complex. Structure-activity-relationship studies have shown that the N-formylamino-salicylamide group is responsible for most of the binding specificity, and suggested that a low pK_a for the phenolic OH group and an intramolecular H-bond between that OH and the carbonyl O of the salicylamide linkage are important.

Two previous X-ray structures of antimycin bound to vertebrate bc_1 complex gave conflicting results. A new structure reported here of the bovine mitochondrial bc_1 complex at 2.28 Å resolution with antimycin bound, allows us for the first time to reliably describe the binding of antimycin and shows that the intramolecular hydrogen bond described in solution and in the small-molecule structure is replaced by one involving the NH rather than carbonyl O of the amide linkage, with rotation of the amide group relative to the aromatic ring. The phenolic OH and formylamino N form H-bonds with conserved Asp228 of cyt b , and the formylamino O H-bonds via a water molecule to Lys227. A strong density the right size and shape for a diatomic molecule occupies the space between the other side of the dilactone ring and the α A helix. The structure also

contains stigmatellin, confirming the binding mode described previously at low resolution from chicken (PDB entry 2BCC) and later in greater detail from the yeast bc_1 complex structures.

The cytochrome bc_1 complex is an enzyme (E.C.1.10.2.2, ubiquinol:cytochrome c oxidoreductase) that comprises the middle part of the mitochondrial respiratory chain. It is a multi-subunit membrane protein, with 10 or 11 protein chains in mitochondrial forms and 3 or more in bacterial complexes. It always contains the three redox subunits cytochrome b , cytochrome c_1 , and the iron-sulfur protein (ISP); which contain respectively two hemes B , heme C and a Rieske-type Fe_2S_2 iron-sulfur cluster. It catalyzes reversible electron transfer from ubiquinol to cytochrome c coupled to proton translocation across the inner mitochondrial membrane, probably by a mechanism like the "protonmotive Q cycle" (1-4). This mechanism, in the form that is widely accepted today, is described in Scheme S1 of the supplemental materials associated with this report.

The existence of inhibitors specifically binding to and inhibiting the two ubiquinone reaction sites was critical in the elucidation of the Q-cycle mechanism. One of the earliest known (for a review of early work see ref. 5) and most potent (with a K_d on the order of 30 pM) of these is antimycin A (antimycin)¹. Antimycin binds specifically to the quinone reduction site (Q_i site) of the cytochrome bc_1 complex. When bound, the visible-UV spectrum of the high-potential cytochrome b is shifted to the red and the fluorescence of antimycin is quenched,

leading to the conclusion that antimycin binds near the heme b_H ².

Together with British Anti-Lewisite (BAL) or alkyl-hydroxynaphthoquinone (HNQ), antimycin enabled the demonstration of two independent pathways for reduction of cytochrome b by ubiquinol, one sensitive to antimycin and the other blocked by BAL treatment or HNQ, in the "double-kill" experiment (6).

When antimycin is bound, the bc_1 complex exhibits an unexpected inverse relation between the redox poise of the high potential chain (iron-sulfur protein and cytochrome c_1) and that of the b cytochromes, resulting in phenomena coined "oxidant-induced" (7) and "reductant-controlled" (8) reduction of b cytochromes. This is explained in the Q-cycle mechanism (Scheme S1, supp. materials) and in an earlier model (9) by having the b cytochromes and the high-potential chain connected to each of two sequential one-electron steps in the oxidation of quinol at the antimycin insensitive (Q_o) site. In the Q-cycle scheme antimycin blocks the reaction at the Q_i site, at which cytochrome b equilibrates directly with the ubiquinone/ubiquinol couple, masking the oxidant-induced reduction in the absence of antimycin.

Generation of a semiquinone at the Q_i site is expected from the Q-cycle mechanism due to sequential one-electron reduction of quinone there by successive turnovers of the Q_o -site reaction. A semiquinone signal has been observed by epr spectroscopy and it is eliminated by antimycin(10,11), consistent with the predictions of the Q-cycle scheme and its explanation of the effects of antimycin. Thus antimycin could be considered a marker for the Q_i site of the Q-cycle mechanism.

Antimycin dramatically increases the stability of the bovine bc_1 complex in the presence of bile salt detergent taurocholate (12), inhibiting the "cleavage" reaction quantitatively at stoichiometric concentrations. These and other observations (13-16) led to the conclusion that antimycin-binding induces a far-reaching conformational change in the cytochrome bc_1 complex. Dithionite reduction of the complex results in a similar protection against cleavage (12), and affects the apparent cooperativity of antimycin binding (16) suggesting that redox state of cytochrome b may also be coupled to the conformational change. More recent indications of an antimycin-induced conformational change include an effect of antimycin on the sensitivity

of the iron-sulfur protein to proteolytic cleavage (17), and an apparent effect of antimycin on "half-the sites reactivity" of the Q_o site (18).

One model (19) for the reaction mechanism of the bc_1 complex invokes conformational coupling between events at the Q_i site, where antimycin binds, and the Q_o site, where the bifurcated transfer of electrons from ubiquinol to cytochrome b and the iron-sulfur protein must be enforced to maintain proton-pumping efficiency (Scheme S1, supp. materials). After different positions of the ISP ectodomain were observed in crystals and proposed to be involved in the catalytic cycle (20), it was suggested (21,22) that such conformational coupling might prevent the ISP from returning to the Q_o site until the second electron had passed to heme b_H and the Q_i site, ensuring bifurcation.

As yet no indication of a conformational change upon antimycin binding has been reported from the x-ray structures. Thus if it exists it must be a rather subtle change. All the evidence is circumstantial, and perhaps amenable to alternative explanations. For example the effect of antimycin on the stability in bile salts may involve strong binding interactions between the inhibitor and the protein serving to hold together the different parts of the sequence contributing to the binding site more strongly than they would be held together in the absence of the inhibitor, perhaps tying down a loose end to prevent some kind of "unraveling" which may initiate the cleavage reaction. Effects on kinetics or proteolytic cleavage of the ISP could be indirect via the effect of antimycin on the resting redox state of the redox centers or the quinone pool.

In potentiometric titrations it has often been observed that the cytochrome b_{662} (b_{560} in bacteria) species attributed to heme b_H titrates heterogeneously(23-28), with part showing a midpoint potential (E_m) around 150 mv and the rest around 50 mv (in bacterial chromatophores at pH 7). In the presence of antimycin only the low potential component is observed (28,29). In the presence of funiculosin there is only one component, with E_m near that of the high potential component (28,30). If the system is poised so that b_H is partly reduced, addition of antimycin results in oxidation of cytochrome b (23,24). These phenomena have been explained as due to the mechanism by which cyt b_H equilibrates with the Q pool via the Q_i site (24,25,29,31), or alternatively as due to redox interaction between the cyt b heme and quinone

species at the Q_i site (27,28) in which the redox state of one component affects the midpoint potential of the other. If the latter explanation is correct, the possibility that antimycin and funiculosin mimic different redox states of ubiquinone at the Q_i site seems attractive.

Thus there remains a large body of experimental observation concerning antimycin and the reaction at the Q_i site that is not very well explained at present. In the process of unraveling the details of the reaction, and in explaining these diverse observations, it would be very helpful to know how antimycin, funiculosin, and ubiquinone bind to the site. In addition, the Q_i site of fungal and other plant pathogens is an important target for crop protection agents (e.g. cyazofamid, see refs. 32,33). The site is of potential significance in treatment of human disease if species-specific inhibitors can be designed. Thus antimycin has been the subject of numerous structure-activity-relationship studies aimed at understanding the mechanism of the enzyme and at developing powerful new crop protection agents (15,34-39).

Antimycin (Figure 1a) has a head group consisting of 3-formylamino salicylate amidified to a dilactone ring consisting of L-threonine (whose amino group is amidified to the salicylate moiety) and a 2-alkyl, 3,4-dihydroxyvalerate. It is the 4-hydroxy group of the latter that participates in the dilactone, and the 3-OH is esterified by a branched carboxylic acid (acyl side chain). There is heterogeneity in the 2-alkyl group (alkyl side chain) and in the branched carboxylate (acyl side chain), which at least in antimycin A1 has recently been shown to consist mainly of 2-methyl butanoate (40) rather than isovalerate (3-methyl butanoate) as deduced earlier (41,42). High resolution chromatography has resolved commercial antimycin samples into as many as ten different compounds (43).

Early structure-activity-relationship studies have led to the conclusions that the N-formylamino-salicyl group is responsible for most of the binding specificity, and to the importance of a low pKa for the phenolic OH group (15). The dilactone ring and substituents can be replaced by a long-chain fatty amine with retention of tight (μ M) binding and inhibition. More recent studies have examined stereospecificity of the dilactone (35) and probed with substituents at various positions on the salicylamide group (36,38). Conclusions of the latter studies include the importance of the phenolic OH and formylamino groups and an

intramolecular H-bond between the phenolic OH and the carbonyl O of the amide linkage by which the rest of the molecule is connected to the 3-formylaminosalicylic acid.

Antimycin was instrumental in locating the Q_i site in the first crystal structure of a bc_1 complex (44), but no coordinates for antimycin were deposited in the Protein Data Bank (PDB). Since then two structures have been made available with coordinates for antimycin, PDB entries 3BCC (chicken) and 1NTK (bovine). The low resolution of the former structure made it impossible to discern details required for a rigorous description of antimycin binding. Structure 1NTK was processed at higher resolution (2.6 Å), however the work presented here shows that it, too, has errors in the details of binding.

In this work we introduce two new crystal structures of the bovine mitochondrial bc_1 complex with stigmatellin at the Q_o site. PDB Entry 1PP9 (2.23 Å) has no Q_i -site ligand added, while 1PPJ (2.28 Å) was co-crystallized with antimycin. This allows us for the first time to reliably describe the binding mode of antimycin at the level of detail required for understanding its diverse effects on the bc_1 complex.

MATERIALS AND METHODS

Bovine hearts were obtained from a slaughterhouse or meat market and either used fresh or stored at -20°C or below before use in the mitochondrial preparation. "Sol-grade" dodecyl β -D-maltopyranoside (DM) and "anagrade" hexyl- β -D-glucopyranoside (HG) were purchased from Anatrace. Stigmatellin and polyethylene glycol (PEG) were from Fluka. Crystallization screen kits mentioned below, as well as cryocrystallography supplies, were from Hampton Research.

Mitochondrial protein was determined by the Lowry method (45) with bovine serum albumin as a standard. Cytochrome bc_1 concentration was determined from the difference in absorbance of the dithionite-reduced sample at 562 vs 600 nm, for which an extinction coefficient for the bovine enzyme of $70 \text{ cm}^{-1}\text{mM}^{-1}$ (E. Berry, unpublished; based on pyridine hemochrome analysis) was used.

Protein purification- Purification was as described (46), involving solubilization of mitochondria with 1.0 g DM per gram protein,

anion exchange chromatography on DEAE Sepharose CL6B with a gradient from 260-500 mM NaCl (in 50 mM KPi buffer pH 7.5, 0.5 mM EDTA, 0.1 g/l DM) and size-exclusion chromatography on Sepharose CL-6B in "sizing buffer" (20 mM K-MOPS pH 7.2, 100 mM NaCl, 0.5 mM EDTA, 0.1 g/l DM). Pooled fractions from the last column were adjusted to 5 μ M cyt *bc*₁ by ultrafiltration or dilution in the same buffer. Stigmatellin and Antimycin A were added to 10 μ M (2-fold molar excess) from 10 mM and 15 mM alcoholic stock solutions.

Before setting up crystallization droplets a final step (PEG fractionation) was carried out in which the inhibitor-loaded *bc*₁ complex was mixed with successive portions of a precipitant solution containing 100 mM KMES pH 6.4, 100 g/L PEG 4k, and 0.5 mM EDTA. This procedure clearly separates two populations, a minor fraction ("aggregated material") which usually precipitates at around 0.3 volumes of precipitant and contains all of the contaminating cytochrome oxidase (present as supercomplex or micelles containing two separate complexes, and incompletely separated by the size-exclusion column) from the major fraction which usually does not begin to precipitate until more than 0.6 volumes have been added. In the case of the antimycin-containing crystal, material precipitating between 0.29 and 0.76 volumes of precipitant was collected by centrifugation and redissolved in several times the original volume of the above-mentioned sizing buffer. To reduce NaCl and residual PEG from precrystallization, the buffer was exchanged by several cycles of dilution in final buffer (20 mM Tris-HCl pH 7.5, 0.5 mM EDTA, 1 g/L UDM) and ultrafiltration on Amicon YM-100 membrane. It is very difficult to dissolve the PEG-fractionation pellet directly in a small volume of final buffer—perhaps due to residual PEG it is necessary to have a higher ionic strength, provided by NaCl in the sizing buffer.

Crystallization- Crystallization was by sitting-drop vapor diffusion. Protein in the final buffer described above was mixed with 0.15 volume of 2.5 M HG, and then one volume (usually 10 μ l) of this detergent-supplemented protein was mixed with 0.9 volume of major precipitant and 0.1 volume of minor precipitant/additive. The major precipitant consisted of 60 g/L PEG-3350, 100 g/L glycerol, 100 mM Na-cacodylate pH 6.7, 20 mM MgCl₂, and 3 mM NaN₃, and the minor precipitant/additive was Hampton

Research's "Screen II #31", consisting of 200 g/L Jeffamine M600 in 0.1 M HEPES pH 7.5.

We calculate the final pH to be about 6.86, ignoring buffering by the protein itself. The ionic strength is 72 mM before vapor diffusion. The droplets were allowed to equilibrate by vapor diffusion against a reservoir containing the major precipitant.

Data collection- The crystals were mounted in a nylon loop on a magnetic pin (Hampton Research) and flash-cooled in liquid nitrogen for cryogenic data collection. The diffraction limit and the cell parameters were highly variable, and in some cases warming the crystal to room temperature for 1-2 minutes and refreezing in the cold stream improved the diffraction dramatically. This seems to be related to the extent of dehydration of the crystals, and we are currently working on a way to optimize the diffraction by systematic dehydration.

The crystal from which structure 1PPJ was obtained was mounted in a loop and dipped in a mixture containing equal parts of the mother liquor and cryoprotectant (250 ml/L glycerol, 120 g/L PEG 4k, 10 mM K-MES pH 6.7, 3 mM Azide) before freezing in liquid nitrogen. After a preliminary exposure revealed diffraction to 4 Å and space group P2₁2₁2₁ with cell parameters 152 × 178 × 227, the pin was removed from the cold stream and set, base down, at room temperature, so the crystal in the loop was dehydrated by the downdraft produced by the cold copper pin. After 3 minutes the pin was returned to the cold stream for data collection, now with resolution limit 2.0 Å and cell parameters 128, 169, 232.

The crystal for structure 1PP9 (without antimycin) was not intentionally dehydrated, however it was one of only 2 crystals diffracting to around 2 Å from about 40 that were mounted from the same well. It is likely that these two crystals were exposed to air longer than the others before freezing. The cell parameters for 1PP9 are somewhat intermediate between the before and after parameters for 1PPJ, suggesting it is less dehydrated. The other crystal from that well diffracting to 2.0 Å had essentially the same parameters as 1PPJ. (This crystal, which we call Y25, will be mentioned again in the context of antimycin-induced structural changes).

Diffraction patterns were collected in 0.5° rotations. Even for the best diffracting crystals, the mosaic spread was large (1.0-1.5°). In order to reduce the data to 2.0 Å without excessive overlap, it was necessary to assume a lower

mosaic spread (0.6°) during spot integration. This results in sampling spot intensity near the maximum of the rocking curve ("profile peak sampling") but ignores tails of the measured reflection's rocking curve as well as overlap from tails of neighboring spots in reciprocal space. This together with radiation decay described below contributes to the higher than usual R-merge and R-sym values for these datasets.

Both crystals used in the present work were rod-shaped, with dimensions $\sim 0.2 \times 0.2 \times 1.5$ mm. This allowed collecting several different datasets from each crystal, at different positions along the long axis of the crystal. It was later determined that significant radiation damage occurred during data collection as indicated by increasing B-factor. In the case of the antimycin-containing crystal (1PPJ), the final dataset was constructed by merging early data from each individual dataset, with a cutoff when the B-factor for scaling against a particular reference was more than 15 \AA^{-2} greater than that for the first exposures. The measurements from these selected frames from each data collection were individually scaled and merged in scalepack. The resulting incomplete datasets were merged together using scalepack to make the final dataset. The statistic R_{merge} in Table 1 and in the PDB file header refers to the R-merge obtained at this second merging step. For structure 1PP9 data from a single collection was used and R_{merge} in Table 1 (R_{sym} in the PDB entry) refers to the initial merging of frames within the dataset.

To prepare for cross-validated (cv) refinement (47) a test set of reflections ("Free-R flags") was chosen from an ideally generated complete dataset to 1.8 \AA , randomly selecting 5% of the reflections. This set of Free-R flags was used with every dataset from this crystal form to avoid biasing the cross-validation.

Structure determination.

Phasing- The first (low resolution) dataset from a crystal of this new orthorhombic form was solved by molecular replacement using PDB entry 1BE3 as model. The iron-sulfur protein was repositioned as in entry 2BCC, and several regions that were observed not to fit the $2F_o - F_c$ density map were rebuilt (significant differences will be discussed in another communication). As successively higher resolution datasets were collected, they were phased by molecular replacement using the best available previous

structure from the same crystal form. Variation in cell parameters made rigid body refinement of the previous structure against the new data unreliable for positioning the molecule in the cell.

For each crystal cycles of manual rebuilding using the graphics program O (ref 48) alternating with rigid body, multi-rigid-body, positional, and restrained atomic B-factor refinement in CNS (49) were used to improve the model. When significant improvement was achieved in one crystal, the appropriate changes were transferred to the other crystals by refining the improved model to convergence against the other datasets, comparing atomic positions with the previous models for those datasets, and examining the differences in the density to decide which model was appropriate on a crystal-by-crystal and residue-by-residue basis.

Non-crystallographic symmetry- The crystal contains a dimer of the bc_1 complex in the asymmetric unit. Initially non-crystallographic symmetry restraints were used for all protein atoms. During rebuilding to fit the electron density it became clear that certain residues did not obey NCS, and the restraints were released for those residues. For a while NCS restraints were eliminated, and the two monomers were refined and rebuilt independently. The resulting structure was examined to locate areas that seemed to violate NCS, and restraints were re-applied everywhere else. The remaining NCS violations were examined to determine whether the electron density supported the violation.

If not, the residue was rebuilt in both monomers to be consistent with NCS and the restraint was reimposed. If the NCS violation appeared real, the surrounding was examined for explanations in the form of crystal contacts. Except in the case of clear NCS violations, application of NCS restraints invariably improved the R-free statistic. It is not known, however to what extent this is due to improvement in the ratio of (data + restraints) to parameters, and to what extent to communication between the test and working sets of reflections (bias) due to the NCS relationship.

In addition to specific violations of NCS, subtle distortions of the protein between the two monomers were present, presumably due to intrinsic flexibility of the protein and the different packing forces. To allow for this flexibility without greatly increasing the number of parameters being fit, the NCS-restrained residues were divided into about 49 NCS groups

each of which was allowed its own NCS operator.

Solvent- Water molecules were added with the water_pick program of CNS, and refreshed periodically by removal of waters flagged by whatcheck as too far from protein and picking of new waters. As the density improved, some of the solvent molecules took on distinct oblong or trigonal shapes, and some of these were modeled as oxygen or azide and glycerol, respectively. Phospholipid and detergent molecules appeared in varying states of disorder, and some of the best have been modeled.

Validation- The refined structures were subjected to validation using procheck (50), sfcheck (51) and whatcheck (52). Residues flagged as unusual were examined and in many cases rebuilt, then the refinement was repeated before testing again. ARP/wARP version 6.0 was used to eliminate model bias and confirm the well-determined parts of the structure by automated rebuilding from free atoms refined by the ARP/wARP (53) process "automated model building starting from existing model". ARP/wARP was able to trace the protein in as few as 53 chains containing over 3700 residues, as compared to 20 chains containing ~4020 residues in the final models. No attempt was made to "dock" the sequence to the traced chain at this time.

When these steps ceased to yield further improvement, the structure was prepared for deposition as follows. No manual manipulation was performed on the final refined structure. Cross-validated refinement statistics for deposition were obtained by the "xtal_pdbsubmission" routine of CNS. The model was then submitted to a final round of non-cross-validated refinement (positional and B-individual) using all the data, with all parameters the same as during the final cv refinement. After a final validation run (sfcheck and procheck as included in the ADIT deposition software on the PDB website; results available in supplemental materials), the coordinates and data were deposited in the PDB.

RESULTS

Resolution and quality of the structure- The diffraction was somewhat anisotropic, as judged by the "falloff" analysis in the program TRUNCATE and by anisotropic scaling during refinement in CNS which gave a B tensor with diagonal elements -15.3, 0.6, 14.7 Å² for 1PP9 and -12.5, 3.8, 8.6 Å² for 1PPJ. The data

reduction and refinement programs we used have no provision for an ellipsoidal resolution cutoff, so to avoid losing any useful data in the well-ordered directions we used a resolution cutoff of 2.07 for 1PP9 and 2.0 for 1PPJ in the initial data reduction. In the final refinement for deposition and calculation of refinement statistics, a resolution limit of 2.1 Å was used for both structures. This should not be taken as the resolution of the structure, however, as the data in the outer shells was quite weak. A more objective measure of the resolution of a diffraction dataset (54) is given by the "optical" resolution (51) as calculated by the program SFCHECK. However the optical resolution is defined differently (as how close two features can be and still be resolved by the data, rather than as a d_{\min} cutoff), so they are not directly comparable. We made a sparse random survey of structures deposited with data during 2002 and found that in the range from 1.2 to 3.0 Å the optical resolution R_{opt} was related to reported resolution d_{\min} cutoff by: $R_{\text{opt}} = 0.42 + 0.59d_{\min}$. The datasets for structures 1PP9 and 1PPJ have optical resolution 1.72 and 1.75 (see sfcheck reports in supplementary material). By the above relation this is the type of resolution to be expected from the average structure using a resolution cutoff of 2.23 or 2.28 Å.

While this is only marginally higher resolution than the best yeast or bovine *bc₁* structures currently available, we think the quality of the structures is significantly higher. This is due to the presence of a dimer in the asymmetric unit, which for the same solvent content doubles the number of unique reflections at a given resolution. Because non-crystallographic symmetry was quite good for the vast majority of the protein, the use of NCS-restraints allowed effective doubling of the data/parameters ratio and improves the behavior of the refinement process. In addition, while making the final model we had the benefit of using all the previously deposited structures for comparison and evaluation, which we gratefully acknowledge.

At the current state of refinement (Table 1b) the free-R factor is approximately 0.40 in the shell around 2.1 Å for 1PP9, and below 0.4 at 2.0 Å for 1PPJ, suggesting the datasets actually contain some useful information to these resolutions. Analysis of the structures by PROCHECK (50,55) show them to be within the norm or better on all measures as compared to 2.0 Å structures. These structures are the first

cytochrome *bc₁* structures to achieve greater than 90% of the residues in the allowed regions (A, B, L) of the Ramachandran plot, as expected for real proteins based on analysis of structures solved at better than 2 Å with R-factors below 20% (ref 50, see ProCheck report in supplemental material). Overall real-space R-factors are 0.155 and 0.148, and real-space correlation coefficients are 0.909 and 0.921 for structures 1PP9 and 1PPJ, respectively (EDS website, URL given below). Representative electron density from various regions in crystal 1PPJ are shown in stereo pairs of Figure 2 as well as the figures documenting the mode of antimycin binding (Figures 1b and c, 7, and 8).

Still, the current structures are disordered in certain regions, and so for some features it will be best to look at structures from other crystal forms. The electron density has been interpreted liberally to provide our best guess of the actual structure in areas where it is not completely determined by the data. To avoid over-interpretation of the structure and possible erroneous conclusions concerning features not described in the text, it is important to compare all the available structures, and to examine the electron density on which the feature is based. To facilitate independent evaluation of structural features by others, we have deposited the original data (structure factors) for all our structures, as recommended by the PDB, IUCr and NIH. For those not set up to do crystallographic computing themselves, there is an "electron density server" website (<http://fsrv1.bmc.uu.se>) which allows one to browse maps for any structure in the PDB using a java-enabled web browser, or check the real-space R-factor and correlation coefficient for a given residue.

Overall Structure- The overall structure of the eukaryotic *bc₁* complex has been described previously (20,44,56,57). The transmembrane region is made up of 26 transmembrane helices, with each monomer contributing 13: 8 from cyt b and one each from subunits 7, 10 and 11 plus the transmembrane anchor helices of the ISP and cyt *c₁*. The redox-active ectodomains of the ISP and cyt *c₁* together with subunit 8 (acidic "hinge protein") make up the membrane extrinsic portion on the external or "P" side of the membrane, while the two largest subunits ("core" proteins (58)) and subunit 6 make up the extrinsic part on the "N" side. Subunit 11 is peripherally bound and readily

dissociable after solubilization in DM. It is not present in this crystal form.

Table 2 lists the number of residues modeled for each subunit for each monomer of the two structures discussed here. It also defines the chain letters for the 10 subunits in each of two monomers: Chains A to J are subunits 1 to 10 of the "first" monomer, while N to W are the corresponding subunits in the second monomer. Reference to this table will facilitate interpretation of the shorthand designation for a residue used here, by which "P:Tyr155" denotes Tyr155 in the third subunit (cytochrome b) of the second monomer. The hemes and iron-sulfur clusters are numbered starting at 501 in the same chain to which they are attached. Water molecules are numbered starting at 1, ligands present at the same place on both monomers are labeled starting at 2001 for monomer 1 and 3001 for monomer 2, and ligands without symmetry mates are numbered starting at 4001.

The 11-subunit bovine *bc₁* complex contains 2166 residues per monomer ((59), Table 2), and the 10-subunit preparation used here has 2110 of these. Due to omission of disordered areas, the final structures contains about 2009 residues in each monomer, or 95% of the residues present. The model is lacking the first 17 residues of subunit 2, the first 14 residues of cytochrome b, the first 11 of subunit 6, the first 12 of subunit 8, about half of subunit 9, and smaller sections elsewhere. Monomer 1 of 1PPJ has fewer residues because it is lacking the first 29 residues of subunit 10, which were disordered. Monomer 2 of 1PP9 contains an additional 5 residues on the N-terminus of cytochrome b; however these are based on the position of these residues in other crystals and not well supported by the density here.

Modeling of the lipids and detergents in these structures is not yet complete, and will be described in a later paper. At present there are five phospholipids in 1PP9 and four in 1PPJ. One of the best ordered (residues 2007 and 3007; with phosphate H-bonding Tyr103 and Tyr104 of cyt b) is in the position of one of the lipids in the chicken *bc₁* structures (e.g. 2BCC) and is also conserved in the yeast *bc₁* complex (1KB9, 1P84). Phospholipids 2006 and 3006 correspond to the "interhelical lipid" described in the yeast *bc₁* complex (57), at the coming-together of transmembrane helices from subunits 3, 4, 5, and 10. As described also by Iwata (60) there are two cardiolipin molecules in the bovine

complex where one was modeled in yeast (1KB9).

A number of hexyl glucoside (HG) molecules have been modeled. For the most part these are poorly ordered and may be misidentified, however in 1PPJ there is one hexyl glucoside that is exquisitely defined by the density (Figure 2b). The hexose ring is pinned in a crystal contact between helix α M of chain A (at the level of 393-394) and the imidazole ring of O:His192 in a symmetry-related dimer, presumably accounting for the good order. In addition there are H-bonds from O2 of the sugar to A:Ser397 (shown) and from O6 to A:Glu394. This well-ordered detergent is seen in all crystals examined so far that have cell edge $a = 128 \text{ \AA}$, but in the looser lattice of 1PP9 this contact does not occur and the detergent is disordered. In one crystal with cell edge $a \sim 120 \text{ \AA}$ (not shown) this detergent is absent and O:His192 of the sym-related molecule packs directly against helix α M⁸ of chain A. Thus the detergent seems to be the "shim" which accounts for the frequent occurrence of the $a=128 \text{ \AA}$ cell edge after partial dehydration of the crystals.

Other observations from the new structure- A detailed description of the new structures 1PPJ and 1PP9, including comparison with other available structures is being prepared. Therefore only some salient features will be mentioned here. As expected in the presence of stigmatellin, the ISP is in the proximal or "b" position, with a hydrogen bond between His161 and stigmatellin, which is bound in cyt. b. The significance of this H-bond has been described in a recent note (61). The methionine sixth ligand in cyt c_I has "R" chirality at the S δ , as in the chicken 1BCC or yeast 1EZV structures (Figure 2a). The heme planes of heme b_H , heme b_L , and cytochrome c_I are at angles of 25 - 26°, 5 - 6°, and 14 - 16° to the membrane normal, respectively (but heme b_H is quite curved, as described below). The orientation of the hemes about their pseudo-two fold axis is unambiguous and is the same as originally modeled in the chicken structure 1BCC. *Cis-* peptide linkages are present at the peptide bonds involving Pro222, Pro436 (cyt b) and Pro74 (cyt c_I) as the (i+1)th residue. The assignment is unambiguous for these three residues, and has been verified in cross-validated SigmaA-weighted F_o-F_c omit maps (available in supplementary materials as Figures 1a, b, and c) calculated for 1PPJ

omitting residues in a sphere of radius 3 Å around the residue and calculated between 93.5 and 2.2 Å resolution. Pro21 in subunit 2 is also modeled as a *cis* peptide, but the position of His20 is not well defined by the density so this is likely to be in error. No other *cis*-peptide linkages were found.

Secondary structure of cytochrome b- The antimycin binding site is entirely within cytochrome b, in contact with the high potential heme b_H . As deduced from hydropathy plots (62-64) and described in previous structures (20,44,57), cytochrome b is primarily α -helical (Figure 3), with eight transmembrane helices labeled $\text{A} - \text{H}$ and four "surface" helices labeled αa (before Helix A), αcd_1 and αcd_2 (Between helices C and D), and αef (between helices E and F). There is one small β -sheet consisting of two antiparallel strands from the linker regions before helices A and E, which will be described below in connection with the antimycin site. The two hemes are located within a four-helix bundle consisting of helices A, B, C, and D; with the high potential heme (heme b_H) toward the N side and low potential heme (heme b_L) toward the P side of the membrane. Both hemes have bis-histidyl ligation, with the histidine ligands provided by helices B and D (His83, 97, 182, and 196 in the bovine sequence). In addition there are four conserved glycines in helices A and C where the heme ring makes a close contact (Gly34, 48, 116, and 130).

Heme b_H and its binding site- Heme b_H , with axial ligands His97 and His196, is distinctly curved with pyrole rings A and C bending toward the His97 side while rings B and D are nearly in a straight line with the iron (forming the axis of curvature). Pyrole rings B and D lie along the axis of the four-helix bundle with rings A and C on the sides; ring C between helices B and C and ring A between helices A and D and contributing to the antimycin binding site (below).

The bonds from the heme iron to the imidazole axial ligands are nearly colinear, with N-Fe-N angle in the range 173.9° to 178.1°. The imidazole bonds, both from N ϵ to iron and from N δ to hydrogen bond partners (described below), are within the plane of the imidazole for both histidines, and presumably serve to fix those planes. His196 has its plane intersecting the heme plane along the line between heme atoms CHB and CHD, 47° from the NA-NC vector. The plane of His 97 is rotated 163° from the

NA-NC vector of the heme, lying approximately along the line between atoms C1C and C1A. The angle between the projections of the two imidazole rings on the heme plane is 145° , breaking the pseudosymmetry of the heme macrocycle and its electronic structure.

As reported (20,57) the propionate on the **A** ring is bent sharply back toward the axial ligand H97, making an ion-pair with the guanidino group of Arg-100 (bovine sequence numbering). We can see now (Figure 4) that this ion pair involves only one of the carboxylate oxygens and NH1 of the guanidino group of R100 (distance 2.8 Å), but that the propionate in addition binds two extremely well-ordered water molecules (Figure 4 and Table 4). The same propionate oxygen that ion-pairs with R100 has a second bond (2.8 Å) to an entity modeled as water W4, B-factor 28 \AA^2 and $2F_o-F_c$ density 5.8σ , whose other ligands are the other (**D**) propionate and Ser205 O γ . The other oxygen of the **A** propionate is separated by 3.3 Å from the NH2 atom of Arg100, but makes a very strong (2.44 Å) bond with another stable (B=29, density 3.3σ) water molecule **W5** which bridges between this propionate and the N δ atom of the heme axial ligand His97. This water also makes bonds with the carbonyl oxygen of Trp30 and backbone N of C33 in the **A** helix. This rigid framework presumably serves to fix the plane of the heme-ligand histidine, and may be partly responsible for the heme curvature mentioned above. Both the water and the Fe atom are approximately in this plane. The sharply bent propionate arm also forms one surface of the **Q_i** binding site (see below), and may be on the path for electron transfer between heme **b_H** and quinone at that site. The other propionate, on the **D** pyrrole ring of heme **b_H**, H-bonds with one carboxylate to the side chains of Ser106 and Trp31, and with the other oxygen to the backbone nitrogen of Asn206 and to the water molecule W4 mentioned above. This arrangement of the propionates, Arg100, the two waters, and their ligands is the same in the presence or absence of antimycin, and is seen also in the yeast **b_{c_I}** structures (e.g. 1P84), so it is likely to be a static arrangement. However we should not rule out the possibility that at some point in the reaction cycle the **A** propionate could be released to straighten out, which would put the carboxylate in the **Q_i** site as a possible ligand for a quinone species there as well as modulating the charge density near the heme

iron and curvature of the macrocycle. Ser205, one of the ligands for strongly ordered water W4, is replaced by Asn221 in *Rb. sphaeroides*. It has been proposed that the O δ 1 atom of Asn221 occupies the position of W4 bridging between the two heme propionates, positioning the N δ 2 atom to serve as a ligand for quinone in the bacterial complex (31).

On the other side of the heme ring, the other axial ligand for **b_H**, His196, appears to form an H-bond (2.90 Å) between its N δ and the backbone oxygen of Thr112. This oxygen is in the plane formed by the imidazole ring and the iron atom. Assumption of a hydrogen bond here requires that His196 is protonated, with implications for the net charge on and redox potential of the heme. Likewise if the water W5 ligating N δ of His97 is an H-bond donor to the propionate and to a backbone carbonyl, then the imidazole N δ must be protonated; implying a positive charge on this imidazole as well.

Molecular configuration of bound antimycin-
The antimycin in structure 1PPJ is very well ordered, with average B-factors in the two monomers of 41.5 and 43.6 Å², barely above that for the backbone of cytochrome b (39.0, 40.9) and lower than the average b-factor for the structure (50.2 Å²). The electron density is correspondingly good, and there is little ambiguity in the placement of any of the atoms except the tips of the alkyl and acyl side chains. The degree of order is greatest on the formylamino-salicylamide portion, which is well defined in $2F_o-F_c$ maps contoured at 2.1 σ (Figure 1b), and decreases through the dilactone ring and into the alkyl and acyl side chains at the other end. At 1.5 σ (not shown) the acyl chain is visible through C3 and shows the methyl branch to be at the 2 position as reported (40) rather than the 3 position as previously believed, and at 0.9 σ (Figure 1c) there is weak density for C4 in one monomer. This C4 carbon of the acyl group has not been modeled in the deposited structure. It is included in Figure 5b and c for completeness, but should be regarded with skepticism. The alkyl side chain has density through the fifth carbon when contoured at 0.9 σ (Figure 1c)

The dihedral angles of the formylamino group are approximately 0° (Θ 1) and 180° (Θ 2), in agreement with values found in an energy-minimized structure (36, which see also for definition of angles). Similar values were found in the small-molecule structure (40) and for the

bound inhibitor in structure 1NTK. These angles put the formylamino group in the plane of the salicyl ring, directed away from the OH and carboxylate groups and toward Lys227 of cyt b. The observation (38) that a methyl group at position 4 but not at position 5 diminishes binding of antimycin analogs is consistent because the methyl at position 4 (their compound 17) would prevent the formylamino group from taking on this conformation (36).

The dihedral angle Θ_3 between the phenyl ring and carbonyl carbon of the salicylate moiety is approximately 180° ; that is the amide group is rotated 180° relative to the salicyl ring from the small-molecule structure. This means that the internal H-bond between the phenolic OH and amide carbonyl oxygen, which was proposed to be important for inhibition (36), and which was observed in the small-molecule structure (40), is actually not present in the enzyme-bound form. The observed orientation of the amide moiety with respect to the salicylate ring is contrary to that modeled in structure 1NTK. This and other discrepancies will be considered in the "conclusions" section.

The 9-membered dilactone ring of antimycin is puckered with alternating members directed up and down except $C\beta$ of the threonine, which is between members facing up and down. The chirality of the chiral centers meshes with the puckering in such a way that the three bulky substituents as well as one methyl side chain ($C5$ of the valeric acid moiety) project equatorially, i.e. more or less in the plane of the dilactone ring, while the two carbonyl oxygens project perpendicular to the ring. The other methyl group ($C\gamma$ of threonine) projects at an intermediate angle. The planes of the ester and amide substituents and the salicyl ring are nearly perpendicular to the dilactone ring. This differs from the small-molecule structure, in which the plane of the salicyl ring and amide are approximately 45° from that of the dilactone ring (Compare Figures 1a and 1b; in both of which the salicylamide is in the plane of the paper).

The antimycin-binding site- Figure 5 shows the make-up of the antimycin binding site in different levels of dissection, and Table 3 lists contacts between antimycin and the protein. The pocket in which the antimycin headgroup is found is bounded by helices αA , αD , αE , and αa ; as well as the edge of heme b_H exposed

between helices αA and αD of the four-helix bundle. Strong hydrogen bonds are formed directly with Asp228 in helix E and via ordered water molecules to Lys227 in Helix E and Ser35 in Helix A .

Figure 5a shows the underpinnings of the antimycin binding site in helices A and E . These helices cross at an angle, with Van-der-Waals contacts at the crossing between the side chains of Leu43 and Leu239 (not shown). The N-terminal (N-side¹) ends of these helices are connected by β -bridges between residues in the sequence preceding the helices: residues 21, 23, and 25 in the region before helix A with residues 221, 220, and 218 before helix E . In addition a strong hydrogen bond between the side-chains of Asp216 and Ser25 hold these two residues together. These beta-bridges are represented by the antiparallel arrows in the cartoons of Figures 3 and 5, and together with helices A and E they bound a triangular volume that encloses the Q_i site (Figure 5). Another connection between the A and E helices is made by Lysine 227 in the E helix which H-bonds with the backbone oxygen of residue 27 and a highly ordered water molecule attached to helix A . These bonds are part of a more extensive H-bonding chain that is involved in antimycin binding but is present in both structures 1PPJ (with antimycin) and 1PP9 (without). This chain is shown in stereo in Figure 5a and schematically, including the bonds to antimycin, in Figure 6. Lys227 and the first water ($W1$) are bonded to each other and to the carbonyl oxygen of residue 27. $W1$ is also bonded to $O\gamma_1$ of Asn32. $N\gamma_2$ of this residue H-bonds a second water ($W2$) which in turn bonds to the carbonyl oxygen of Asp228 and Ser35 $O\gamma$, further linking the A and E helices. A third water ($W3$) also bonds with Ser35 $O\gamma$ and additionally with the backbone O and N of residues 31 and 35, respectively (Figure 5a). As these latter two atoms would normally be involved in the α -helical H-bonding of helix A , $W3$ can be seen as "intercolated" into the helix. In fact the helical bonding is interrupted, with normal α -helical bonding involving the N atom of residues after 35, 3/10 helical bonding involving the O of residues before 31, and no strong helical bonds of either sort involving O of residue 31 or 32 and N of residue 35. The distance from 31 O to 35 N is 5.1 Å, and to 34 N 4.1 Å. The intercolated water $W3$ is well ordered, with B-factors 25 and 32 Å² in 1PPJ (but 30 and 46 Å² in 1PP9), well below average

for the structure, and with density in $2F_o - F_c$ maps 3.9 to 4.7 σ . The heme-propionate-to-axial-ligand-bridging water W5 mentioned above can also be seen as intercolated, with a close H-bond to 33 O, but it is equally close to 33 N and 34 N, with neither being as close as 35 N is to W3 (Table 4). Figure S1 in supplemental material illustrates the interaction of these two waters with the helical backbone atoms.

As mentioned above both the **D** helix and the α -a surface helix contribute to the Q_i site. Helix **D** is omitted in 3a and 3b for clarity (the view is from the position of helix **D**), but the linker polypeptide connecting helix **D** to helix **E** is shown, as is the N-terminus of cytochrome **b** starting with residue 15 in the α -a helix. Ser205, early in the **D/E** linker is shown as ball-and-stick. This residue has been implicated in quinone binding at this site (31,57,65,66). Residue 16 at the end of the α a helix is also shown as a marker for this region that forms part of the wall of the Q_o site.

Figure 3b introduces antimycin and heme b_H , and Figure 3c shows everything represented in 3b as spacefilling model and introduces helix **D** as a thin ribbon. The H-bonding contacts of antimycin can be seen in Figure 3b and, in greater detail in Figures 6-8. The only direct H-bonds with the protein involve conserved Asp228, the carboxylate of which H-bonds to the phenolic OH and the formylamino NH^6 . It seems reasonable to assume that Asp228 is deprotonated at the pH of the crystal, and serves as H-bond acceptor in both these bonds. The phenolic OH also has an H-bond with the intercolated water W3, as well as the intramolecular H-bond mentioned above with the amide NH. Following the reasoning above it must be the acceptor in both of these bonds, as its one proton is being donated to Asp228.

The substituents of the "A" pyrole ring of heme b_H (the bent propionate described above and a methyl group) protrude from the 4-helix bundle between the **A** and **D** helices, forming part of the surface of the Q_i site. The space-filling model in Figure 3c illustrates the intimate contact between heme (orange) and antimycin (magenta), consistent with the electronic interactions required to explain the quenching of antimycin fluorescence and the spectral shift of cytochrome b_H on binding. The aromatic headgroup of antimycin is inserted into a cavity between the bent propionate and Phe220. The aromatic ring of Phe220 is not quite

perpendicular to the salicyl ring, the actual angle being 77° . The axial methyl group of the dilactone ring interdigitates loosely with the methyl groups on pyrole rings **A** and **B** of the heme.

Van der Waals contact with Ser205- On the other side of the Formylamino-salicyl ring from Asp228, potential H-bonding partners are Ser205 and His201 (Figure 5b and c, Figure 8), both believed to be important in ubiquinone binding at the Q_i site (31,57,65,67). Ser205 makes Van-der-Waals contact with C5 of the salicylate ring, but there is no H-bonding partner on this area of antimycin. In antimycin analogs lacking the 3-formylamino group, inhibition can be restored by 3- or 5- NO_2 groups, and to some extent by a 5-formylamino group (39). This has been attributed to a requirement for an electron-withdrawing substituent to increase the acidity of the phenolic OH (15), however, based on a more extensive set of analogs, Tokutake et al decided that electron-withdrawal did not correlate well with activity, and concluded specific interactions of both the formylamino and phenolic OH with the protein were involved. It seems likely that a nitro group in the 5-position would H-bond Ser205, while one in the 3- position would H-bond Asp228. Superposition of 3- or 5-nitrosalicylate on the salicylate moiety of antimycin in 1PPJ (not shown) results in too-close contacts (1.7 and 1.3 Å) of the 3-nitro group oxygen with Asp 288 and the 5-nitro group with Ser205. Small adjustments in the positions of these side chains, or slight repositioning of the ring, could allow a good fit.

Thus H-bonding may be as important as electron-withdrawal in explaining the effects of nitro- substituents. However in light of our assumption that the phenolic OH is the H-bond donor in the bond with Asp228, it has to be questioned whether the more acidic nitro-compounds, which might be deprotonated at neutral pH, could bind in the same way as antimycin. In fact the detailed inhibition pattern of nitrosalicylate compounds has been found to be quite different from antimycin and other 3-formylamino compounds, the nitrosalicylates being ineffective in eliciting either the double-kill behavior or oxidant-induced reduction seen with antimycin (38,68).

His201 conformation- The most enigmatic part of the structure around the antimycin binding

site is the critical conserved residue His201 which is believed to be a ligand for quinone (57,65,67), either directly (65) or indirectly through a water molecule (57). When contoured at a 1.5σ density level (Figure 8a) the imidazole ring seems well localized, but not as shapely as expected at this resolution. His201 here is modeled in a position close to rotamer 5⁴, as in all vertebrate cyt *bc*₁ structures currently available, and there is really no possibility of modeling it in with a significantly different value of chi-1.

The distance from His201Ne2 to the antimycin O is 4.20 Å, precluding any significant direct H-bonding. An extra bit of density has been modeled as water, with distances 2.81 Å from the water to the amide carbonyl O of antimycin and 2.63 Å to the Ne2 of His201. In fact the density is too close to the histidine to be a water molecule. Non-bonded interaction terms in the refinement process have pushed the modeled water outside of the density peak, and displaced His201 slightly from its best fit. When the water is moved to its density peak, the distances are 1.82 to the His201 and 3.07 to antimycin. When the water is removed and the model is subjected to further positional refinement, His201 moves only slightly closer to antimycin, distance 4.12 Å (not shown).

When contoured at a lower level (1.0σ , Figure 8b), the density around the imidazole spreads out in a triangular shape and merges with the peak assigned to water. Possible explanations are post-translational modification of His201 or, otherwise, a mixture of two alternative situations: one in which the water is present at its density peak but His201 rotates back to be farther from it, and another in which the water is absent and His201 rotates forward toward the water position and bonds directly with antimycin.

The two conformations postulated here, and the presence or absence of a water molecule between the histidine and the Q_i-site occupant, should not be confused with another interesting difference between available structures. In all the yeast structures presented to date, His 202 (corresponding to His201 in the bovine sequence) is positioned close to rotamer 3⁴. A water molecule bridges between the Ne2 nitrogen and the carbonyl oxygen of ubiquinone. In the chicken *bc*₁ structures with ubiquinone, His202 is close to rotamer 5, which allows a direct H-bond to ubiquinone. It seems quite

reasonable that both these conformations are correct, depending perhaps on pH or ionic strength, and that the direct involvement of a water may be part of the mechanism for uptake of the protons involved in quinone reduction at the Q_i site. However that may be, all of the vertebrate *bc*₁ structures available today have His202 (201) in rotamer 5, and all the yeast structures have rotamer 3. At first glance the bovine structure 1NTZ (with quinone supplemented) seems to be an exception, as the H-bond between quinone and His201 is mediated by a water molecule as in the yeast structures. However superposition of the chicken and yeast structures shows that in 1NTZ, His201 is in the chicken position (rotamer 5) and the quinone is deeper in the pocket than in the yeast or chicken structures, making room for the mediating water.

Unknown molecule in hydrophobic site between dilactone and helix A- There is a strong density between the dilactone ring of antimycin and helix, A which during most of the refinement of the structure was modeled as a water. Since there are no nearby H-bonding partners to account for stabilizing a water molecule in this position, it was removed before submitting the structure to the PDB. However this leaves a strong peak in difference Fourier maps, indicating that something is there, even if it is not a water. The peak is oblong and about the right size for a diatomic molecule. In consideration of the hydrophobic nature of the environment and the lack of H-bonding partners we think it may be a nonpolar gas such as nitrogen or oxygen. It is modeled as O₂ in Figure 8, and labeled "unknown". The closest contacts in antimycin are O7 and C11 (3.7 and 4.0 Å). The closest contacts in helix A are the carbonyl O of ser35 (4.0 Å) and sidechains of Ile39 and Ile42 (4.0 - 4.2 Å).

Conformational change induced by antimycin binding and different crystal packing forces- In order to look for conformational changes induced by antimycin binding, we compared C- α positions of cytochrome *b* in structure 1PPJ with structures lacking antimycin (Figure 9 and Table 5). Structure 1PP9 lacks antimycin but has significantly different cell parameters (Table 1a) from 1PPJ, so differences may be due to different packing forces. A third structure of similar resolution (optical resolution 1.70) and lacking antimycin but with cell parameters

similar to 1PPJ was compared to control for these changes.

In the structures compared here (all containing stigmatellin), a core domain consisting of the four TMH of the four-helix bundle plus much of **cd**₁-**cd**₂, the **ef**-linker, and the **F** helix before the kink at 300 (α F1) could be superimposed with rmsd 0.133 Å or below and maximum deviation 0.28Å. The exact residues included in this core are listed in the legend to Figure 9, which shows the by-residue deviation between structures without antimycin compared with 1PPJ when cytochrome b is thus superimposed

The N-terminus and the **de** linker, both involved in the **Q_i** site, were significantly different between 1PPJ and 1PP9, while the **ab** and **bc** linkers showed minor deviations. The mobile region in the **de** loop actually extends into the N-terminal part of helix **E**, as far as residue Lys227.

Helix **E** starting at 228 could be included in the core domain but gave a slight but perhaps significant increase in rms deviation between the C chains of 1PPJ and 1PP9 (but not between P chains). To test the hypothesis that the **E** helix transmits a conformational signal to the P side upon antimycin binding at the **Q_i** site, helix **E** was excluded from the core region used for superposition, and treated as a separate domain.

Such by-residue plots of atom deviation are limited in sensitivity by the inherent noise in the structure, the estimated SD for atom positions being 0.3 - 0.5 Å for these structures (Table 1b). If it is assumed that sections of protein move as rigid bodies, much smaller movements can be detected because positions of all the atoms in the body contribute to determining its position and the "jitter" in individual atomic positions averages out to some extent. We tested two domains for such rigid body movement relative to the core domain used for superposition. One was the helix **F**₂+**G**+**H** region discussed below, which seems to be moving independently between 1PPJ and 1PP9, and the other was helix **E**, which shows significant deviations between these structures in the C chain (Figure 9a). To do this the operator best superimposing the domain in question was compared with the operator superimposing the core domain, giving an operator for the additional movement required to superimpose the domain in question after the core domain has been superimposed. This operator was then expressed as a rotation angle and as the largest

movement of any atom in the domain upon application of the operator. Results are listed in Table 5

Helix **F** after the kink at residue 299 (α F2) together with the **G** and **H** helices form a separate domain which is rotated significantly with respect to the core domain described above: a rotation of 1.3° with maximum C- α displacement (at C378) of 0.81 Å (In the case of C chains of 1PPJ and 1PP9). This is based on determining operators best superimposing the two domains, applying each to 1PPJ, and seeing how far the atoms of 1PPJ move, so does not include jitter in individual atom positions between structures.

As a control to test the significances of the differences observed, the Y21 structure was resolved twice starting with structures 1PPJ in one case and 1PP9 in the other. After positioning the models using the now-well-known intercrystal operators followed by rigid-body refinement and a few rounds of alternating positional minimization and restrained atomic B-factor refinement, the entire cyt b backbone after residue 20 was superimposable with maximum deviation 0.16 Å and RMSD 0.04. This implies that the small differences observed in this region between 1PPJ and 1PP9 are within the radius of convergence of positional refinement, as expected from their small magnitude.

The fact that the differences in cyt b between 1PPJ and 1PP9 disappear when refined against the same dataset assures us that they are real differences in the data and not results of accidental differences in the history of model-building. However the differences correspond more to differences in cell parameters and which of the two monomers in the dimer is being compared than to the presence or absence of antimycin, suggesting they result from different packing forces rather than an antimycin-induced change.

The N-terminus of cytochrome b up to residue 20 is modeled differently in 1PP9 and 1PPJ, to the extent that manual rebuilding would be required for convergence when refined against the same data. Density is not very clear here and it seems likely that multiple conformations exist for all three structures. This region was modeled differently in the bovine cyt **bc**₁ structures from Uppsala (1BE3, 1BGY) as compared to those from Bethesda (e.g. 1L0L). The possibility has been raised (69) that the N-terminus including α -a helix serves to transmit a

conformational signal between Q_i sites of the two monomers.

Stigmatellin binding- Stigmatellin binding has been reported from a number of cyt bc_1 crystal structures (20,57,70) and coordinates have been deposited for two chicken bc_1 structures (2BCC and 3BCC) and for all of the yeast bc_1 structures (e.g. 1KB9). Coordinates have recently been deposited for a bovine structure containing stigmatellin (1SQX), however those coordinates are not available for comparison at the time of this writing. The two chicken structures had stigmatellin bound in opposite orientations. That of the later (2BCC) structure was confirmed by the higher-resolution yeast structures (1EZV and following), and by the structures described here.

The entire stigmatellin molecule is well ordered in the current structures, with all but two atoms (the methoxy carbon C5A and final carbon of the tail) covered by $2F_o-F_c$ density at a contour level of 2.0 σ (Figure 2c). The stereochemistry of the 4 chiral centers and the planarity at the isoprenoid unit are clear, and are consistent with what is known from chemical investigations (71).

The current structures essentially confirm the binding mode reported in the yeast bc_1 crystals except for some details of the "tail". The main polar interactions (Table 6) are an H-bond (2.80 Å) between the carbonyl oxygen O4 and His161 of the iron-sulfur protein and one (2.54 Å) between the ring OH group (O8) and the side chain of Glu271 in the conserved PEWY motif. As in the yeast structure there is a water molecule bridging between O8 and the second carboxylate oxygen of the PEWY glutamate. Another water molecule is bound between that second carboxylate oxygen, OH of the PEWY tyrosine, and the carbonyl oxygen of ALA127, stabilizing the position of the PEWY glutamate for its interaction with the Q_o site ligand and perhaps forming part of the pathway for release of protons upon oxidation of ubiquinol.

The other interactions (Table 6) appear to be hydrophobic and Van der Waals, although the interaction between Tyr278 and the O4 atom of stigmatellin may be a nonconventional H-bond as suggested by Palsdottir et al. (72) in the case of a related inhibitor. The tail of stigmatellin at the level of the first methoxy group passes through a hydrophobic orifice (between helices cd_2 , C, and F) into the bulk lipid phase, then bends sharply and lies against the outside surface. The hydrophobic orifice is bounded by residues Phe274, Met124, Ileu298, Ala277,

Leu294, Leu149, Ile146, and Phe128 (going clockwise around when viewed from outside). On the outside, the tail lies on the surface between helices cd_1 and C, contacting residues 128, 129, 146, 147, 178. The bent tail wraps around the side chain of Ile146 in the orifice, so that atoms C γ 1 and C δ 1 form part of the wall of the binding pocket for the head group, while C γ 2 forms part of the binding surface for the external tail. Presumably the hydrophobic orifice is the entry point to the Q_o site for ubiquinone and hydrophobic inhibitors, and the size and shape of the orifice as much as the binding properties of the site determine what substrates and inhibitors can be accommodated.

Ramachandran outliers- It is normal for well-refined structures even at high resolution to have 1-5% of residues in the "Forbidden" zone of the Ramachandran plot. However a Ramachandran outlier can also be an indication of a misbuilt residue. Therefore we have examined the outliers in the two structures presented here to see how well the conformation presented is supported by the density.

Tyr155 of cytochrome b is a particularly interesting outlier that is well supported by the density. In bacterial bc_1 complexes, there are two conserved glycines in the turn between helices cd_1 and cd_2 , corresponding to positions 155 and 157 in the bovine sequence. Gly157 is also conserved in the mitochondrial complexes, but surprisingly 155 tends to be an aromatic tyrosine in most vertebrates, phenylalanine in yeast. However the backbone phi, psi values for this residue are 66 to 68 and -39 to -42° in the bovine structures and 76.6, -75.0° in the yeast structure. These values lie outside the allowed region on the ramachandran plot for any residue but glycine. Thus a mitochondrial progenitor has placed an aromatic at a position in the fold where only glycine could be accommodated readily, and this strained aromatic has been preserved through evolution. We will not speculate about the function, but note that the αcd_1-cd_2 hairpin helix forms part of the Q_o site, and movement of this helix in response to Q_o -site occupancy or ISP position (73,74) has been reported.

The residue corresponding to Tyr155 is also a ramachandran outlier in all available structures of the chicken or yeast bc_1 complex, and in the bovine complex in tetragonal crystals (e.g. 1L0L). Outlier status is avoided in structures 1BE3 and 1BGY by flipping the plane of the preceding peptide (154-155) relative to all

other structures, however this arrangement of the backbone is completely incompatible with the density in the crystals reported here. The backbone density for this residue is quite strong and unambiguous, however the density on the ring and OH has a peculiar shape. This side chain sticks out into the solvent from the turn of the **cd₁-cd₂** hairpin and makes no contacts with the rest of the protein, so it is not surprising if it is not well ordered.

Residue Ala171 in the second largest subunit also falls in the disallowed region of the Ramachandran plot. This is in a 3-10 helical turn at the end of helix $\alpha\mathbf{D}^8$. The electron density leaves little doubt as to the positions of the atoms, so we believe this also is a real outlier. It is an outlier in the yeast (1P84) and tetragonal bovine (1L0L) structures as well, but not in 1BGY, again as a result of flipping the peptide plane (B170-B171) in a way which is inconsistent with the density in our structures.

Residue Met71 in the "tether" region of the ironsulfur protein differs in the two monomers. The conformation modeled in the first monomer (chain **E**) is an outlier in the structure deposited for 1PPJ (with antimycin), but not in 1PP9 or the Y21 structure, or in chain R of any structure. This residue appears to have several conformations and is not very well-ordered, and further refinement and rebuilding based on the Y21 structure since deposition has resulted in a conformation that fits the density equally well without deviating from the allowed region of the ramachandran plot.

The other Ramachandran outliers are found in poorly defined regions (A223,224 in the interdomain linker of the largest subunit) and probably represent errors in the model.

DISCUSSION

A number of features of the **bc₁** complex revealed by the presented structures and not discerned in previous structures suggests that this is the most accurate structure of the **bc₁** complex available. In particular, the binding mode of the inhibitor antimycin is defined to a high level of accuracy. The new structure is consistent with results of structure-activity relationship studies, however it does not support one of the conclusions from those studies: that the intramolecular hydrogen bond between phenolic OH and carbonyl O described for the molecule in solution (36) and in the small-molecule crystal (40) is important for binding and inhibitory activity. On the contrary,

the bound molecule has the carbonyl oxygen facing His201 with a long, weak, or water-mediated hydrogen bond while the amide nitrogen H-bonds to the phenolic hydroxyl oxygen. This is quite understandable because the phenolic OH group is H-bonding to aspartate and is likely to be the donor in that interaction. This would make an H-bond to the carbonyl oxygen impossible, as that atom can only be an H-bond acceptor. The amide nitrogen, on the other hand, has one proton that would be available for H-bond donation. Such a rearrangement of the H-bonding pattern upon binding is not surprising, in fact the possibility was suggested in the small-molecule structure report (40). The importance of the intramolecular H-bond was suggested by the fact that an antimycin analog in which the amide is separated from the salicylate benzene ring by an extra carbon (compound B of ref 36) and thus could not form the H-bond, was 10⁴-fold less potent than an analogue with the amide directly connected as in antimycin. However this compound would be equally unable to form the intramolecular H-bond between amide nitrogen and phenolic oxygen that we observe in the bound inhibitor, so these experimental results are consistent with our structure. In fact it could be said that our structure supports their conclusion of the importance of an internal H-bond between phenolic oxygen and the amide, but their experiments gave no hint that the amide is flipped and the amide N rather than O is involved in the H-bond.

The structure of bound antimycin and the surrounding protein presented here differs in some significant details from that of the structure 1NTK (66). Most importantly, the conformation of antimycin in the binding site is different. While both structures agree that the dilactone and formylaminosalicylate rings are rotated relative to each other as compared to the small-molecule structure, 1NTK keeps the dihedral between the amide moiety and the FSA fixed, preserving the intramolecular H-bond between the phenolic OH and the amide O. In 1PPJ there is 180° rotation about this dihedral relative to the small-molecule structure, breaking the intramolecular bond and forming a new one between the amide NH group and the phenolic O.

In addition two key residues Ser35 and Lys227 have their side chains modeled differently in the two structures, resulting in

different roles for these residues in antimycin binding. Gao et al.(66) report from structure 1NTK that Ser35 forms H-bonds with the amide carbonyl O and a carbonyl O of the dilactone ring. In 1PPJ Ser35 is in the most stable rotamer⁴, facing away from antimycin (Figure 7a) and H-bonds with two waters (W3, W2) and the carbonyl oxygen of residue 32, but makes no direct H-bond to antimycin. If it were to change to rotamer 2 it would be positioned to H-bond the carbonyl oxygen of the threonine moiety of the dilactone, as in the model of Gao et al. However the electron density (Figure 7a) gives no indication of Ser35 in rotamer 2, even at partial occupancy, or of a water mediating an H-bond to that atom. On the contrary, as described above W3 mediates an H-bond between Ser35 and the phenolic OH of antimycin.

Likewise Lys227N ζ makes a direct bond to the formylamino oxygen of antimycin in 1NTK, but in 1PPJ these atoms are 5.2 Å apart and ordered water W1 binds between them (Figure 7b, 8).

Whenever different results are obtained from two different crystal forms of the same protein under different conditions, it has to be asked whether the different results correctly represent two different states of the protein (possibly corresponding to different steps along a reaction pathway) or whether the feature is actually invariant and one of the structures is in error. In the case of the orientation of the antimycin amide group it seems unlikely that both bonding modes are possible. Unfortunately the 1NTK structure was deposited without supporting data (structure factors), which makes it impossible to test whether the data would have been equally consistent with our current structure. However the density depicted in the stereodiagram of Figure 2A of (66) appears consistent with our structure, having an unaccounted-for protrusion about where we put the carbonyl oxygen, and having the modeled carbonyl oxygen at the edge of contoured density with no surrounding protrusion of the density.

While we want to emphasize that the structure of antimycin in 1PPJ is based on the

electron density from x-ray diffraction by a crystal and not on chemical considerations or structure-activity relationships, the flipping of the salicylate amide moiety relative to the small-molecule structure seen here nicely explains why compound **D** of (36), which is methylated on the amide N, is a poor inhibitor despite still having the internal H-bond (albeit weaker) between phenolic OH and carbonyl oxygen in solution. The amide of a secondary amine cannot be a hydrogen-bond donor, so the intramolecular H-bond that we see between phenolic OH and amide N cannot form, and the methyl group would clash with the phenolic OH preventing the molecule from taking this conformation. The explanation is less obvious with the structure presented in 1NTK, as the amide nitrogen is oriented toward a spacious part of the pocket containing only water molecules that might be expected to be displaceable.

As for the discrepancies regarding the roles of Ser35 and Lys128, it seems more possible that the different rotamers observed in the current 1PPJ structure as opposed to 1NTK represent different states depending on pH or ionic strength. However the failure of that structure to correctly orient the amide linkage weakens the argument for different conformations of these residues. Since electron density was not shown supporting the modeled rotamers, and data are not available for independent evaluation, we hesitate to propose alternate conformations for these residues at this time.

Ser35 is not required for antimycin binding, as *Rhodobacter* and *Paracoccus*, which have Val or Ile here, are inhibited by antimycin. However *R. rubrum* has Ser as in mitochondria, and is more sensitive (in whole cells) than *Rhodobacter* (pers. communication of Fevzi Daldal). Schnauffer et al. (75) found that mutation of Ser35 to Ile led to antimycin resistance in *L. tarentolae*. However the effect of Ser35Ile substitution might be expected due to steric effects, and is not necessarily indicative of a role of this residue in H-bonding to antimycin or stabilizing the waters involved in antimycin binding.

REFERENCES

1. Mitchell, P. (1976) *J Theor Biol* **62**, 327-367
2. Crofts, A. R., and Meinhardt, S. W. (1982) *Biochem Soc Trans* **10**, 201-203
3. Mitchell, P. (1974) *FEBS Lett* **43**, 189-194
4. Trumpower, B. L. (1976) *Biochem Biophys Res Commun* **70**, 73-80.
5. Slater, E. C. (1973) *Biochim Biophys Acta* **301**, 129-154
6. Deul, D. H., and Thorn, M. B. (1962) *Biochim Biophys Acta* **59**, 426-436
7. Chance, B. (1958) *J Biol Chem* **233**, 1223-1229
8. Trumpower, B. L., and Katki, A. (1975) *Biochem Biophys Res Commun* **65**, 16-23.
9. Wikstrom, M. K., and Berden, J. A. (1972) *Biochim Biophys Acta* **283**, 403-420
10. Siedow, J. N., Power, S., de la Rosa, F. F., and Palmer, G. (1978) *J Biol Chem* **253**, 2392-2399
11. Yu, C. A., Nagaoka, S., Yu, L., and King, T. E. (1978) *Biochem Biophys Res Commun* **82**, 1070-1078
12. Rieske, J. S., Baum, H., Stoner, C. D., and Lipton, S. H. (1967) *J Biol Chem* **242**, 4854-4866
13. Van Ark, G., and Berden, J. A. (1977) *Biochim Biophys Acta* **459**, 119-127
14. Baum, H., Rieske, J. S., Silman, H. I., and Lipton, S. H. (1967) *Proceedings of the National Academy of Sciences of the United States of America* **57**, 798-805
15. Rieske, J. S. (1980) *Pharmacol Ther* **11**, 415-450
16. Berden, J. A., and Slater, E. C. (1972) *Biochim Biophys Acta* **256**, 199-215
17. Valkova-Valchanova, M., Darrouzet, E., Moomaw, C. R., Slaughter, C. A., and Daldal, F. (2000) *Biochemistry* **39**, 15484-15492
18. Covian, R., Gutierrez-Cirlos, E. B., and Trumpower, B. L. (2004) *J Biol Chem* **279**, 15040-15049
19. Brandt, U., and von Jagow, G. (1991) *Eur J Biochem* **195**, 163-170
20. Zhang, Z., Huang, L., Shulmeister, V. M., Chi, Y. I., Kim, K. K., Hung, L. W., Crofts, A. R., Berry, E. A., and Kim, S. H. (1998) *Nature* **392**, 677-684
21. Brandt, U. (1998) *Biochim Biophys Acta* **1365**, 261-268
22. Brandt, U. (1999) *J Bioenerg Biomembr* **31**, 243-250
23. de Vries, S., Albracht, S. P., and Leeuwerik, F. J. (1979) *Biochim Biophys Acta* **546**, 316-333
24. Glaser, E. G., Meinhardt, S. W., and Crofts, A. R. (1984) *FEBS Lett* **178**, 336-342
25. Meinhardt, S., and Crofts, A. (1984) in *Advances in Photosynthesis Research* (Sybesma, C., ed) Vol. 1, pp. 649-652, Martinus Nijhoff/Dr. W. Junk Publishers., The Hague
26. Robertson, D. E., Prince, R. C., Bowyer, J. R., Matsuura, K., Dutton, P. L., and Ohnishi, T. (1984) *J Biol Chem* **259**, 1758-1763

27. Salerno, J. C., Xu, Y., Osgood, M. P., Kim, C. H., and King, T. E. (1989) *J Biol Chem* **264**, 15398-15403
28. Rich, P. R., Jeal, A. E., Madgwick, S. A., and Moody, A. J. (1990) *Biochim Biophys Acta* **1018**, 29-40
29. Crofts, A., Barquera, B., Bechmann, G., Guergova, M., Salcedo-Hernandez, R., Hacker, B., Hong, S., and Gennis, R. (1995) in *Photosynthesis: from light to biosphere*. (Mathis, P., ed) Vol. II, pp. 493-500., Kluwer Academic Publ., Dordrecht.
30. Kunz, W. S., and Konstantinov, A. A. (1983) *FEBS Lett* **155**, 237-240
31. Dikanov, S. A., Samoilova, R. I., Kolling, D. R., Holland, J. T., and Crofts, A. R. (2004) *J Biol Chem* **279**, 15814-15823
32. Mitani, S., Araki, S., Takii, Y., Ohshima, T., Matsuo, N., and Miyoshi, H. (2001) *Pesticide Biochemistry and Physiology* **71**, 107-115(109)
33. Ohshima, T., and Komyoji, T. (2004) *J. Pestic. Sci.* **29**, 136-138
34. Dickie, J. P., Loomans, M. E., Farley, T. M., and Strong, F. M. (1963) *J Med Chem* **122**, 424-427
35. Miyoshi, H., Kondo, H., Oritani, T., Saitoh, I., and Iwamura, H. (1991) *FEBS Lett* **292**, 61-63
36. Miyoshi, H., Tokutake, N., Imaeda, Y., Akagi, T., and Iwamura, H. (1995) *Biochim Biophys Acta* **1229**, 149-154.
37. Tokutake, N., Miyoshi, H., Nakazato, H., and Iwamura, H. (1993) *Biochim Biophys Acta* **1142**, 262-268
38. Tokutake, N., Miyoshi, H., Satoh, T., Hatano, T., and Iwamura, H. (1994) *Biochim Biophys Acta* **1185**, 271-278
39. Neft, N., and Farley, T. M. (1971) *J Med Chem* **14**, 1169-1170
40. Kim, H., Esser, L., Hossain, M. B., Xia, D., Yu, C.-A., Rizo, J., Helm, D. v. d., and Deisenhofer, J. (1999) *Journal of the American Chemical Society* **121**, 4902 - 4903
41. Birch. (1961) *J. Chem Soc.* **1961**, 889
42. van Tamelan, E. E., Dickie, J. P., Loomans, M. E., Dewey, R. S., and Strong, F. M. (1961) *J. Am. Chem. Soc.* **83**, 1639-1646
43. Ha, S. T., Wilkins, C. L., and Abidi, S. L. (1989) *Anal Chem* **61**, 404-408
44. Xia, D., Yu, C. A., Kim, H., Xia, J. Z., Kachurin, A. M., Zhang, L., Yu, L., and Deisenhofer, J. (1997) *Science* **277**, 60-66
45. Lowry, O. H., Rosebrough, N. J., Farr, A. L., and Randall, R. J. (1951) *J Biol Chem* **193**, 265-275
46. Berry, E. A., Huang, L. S., and DeRose, V. J. (1991) *J Biol Chem* **266**, 9064-9077
47. Brunger, A. T. (1992) *Nature* **355**, 472-474
48. Jones, T. A., Zhou, J.-Y., Cowan, S. W., and Kjeldgaard, M. (1991) *Acta Crystallogr.* **A47**, 110-119
49. Brunger, A. T., Adams, P. D., Clore, G. M., DeLano, W. L., Gros, P., Grosse-Kunstleve, R. W., Jiang, J. S., Kuszewski, J., Nilges, M., Pannu, N. S., Read, R. J., Rice, L. M., Simonson, T., and Warren, G. L. (1998) *Acta Crystallogr D Biol Crystallogr* **54**, 905-921

50. Laskowski, R. A., MacArthur, M. W., Moss, D. S., and Thornton, J. M. (1993) *J. App. Cryst.* **26**, 283
51. Vaguine, A. A., Richelle, J., and Wodak, S. J. (1999) *Acta Crystallogr D Biol Crystallogr* **55 (Pt 1)**, 191-205
52. Hooft, R. W., Vriend, G., Sander, C., and Abola, E. E. (1996) *Nature* **381**, 272
53. Perrakis, A., Harkiolaki, M., Wilson, K. S., and Lamzin, V. S. (2001) *Acta Crystallogr D Biol Crystallogr* **57**, 1445-1450
54. Weiss, M. S. (2001) *Journal of Applied Crystallography* (**0**). **34**, 130-135
55. COLLABORATIVE COMPUTATIONAL PROJECT, N. (1994) *Acta Cryst. D* **D50**, 760-763
56. Iwata, S., Lee, J. W., Okada, K., Lee, J. K., Iwata, M., Rasmussen, B., Link, T. A., Ramaswamy, S., and Jap, B. K. (1998) *Science* **281**, 64-71
57. Hunte, C., Koepke, J., Lange, C., Rossmann, T., and Michel, H. (2000) *Structure Fold Des* **8**, 669-684
58. Silman, H. I., Rieske, J. S., Lipton, S. H., and Baum, H. (1967) *J Biol Chem* **242**, 4867-4875
59. Schagger, H., Brandt, U., Gencic, S., and von Jagow, G. (1995) *Methods Enzymol* **260**, 82-96
60. Iwata, M. (2001) in *Department of Biochemistry*, Uppsala University, Uppsala
61. Berry, E. A., and Huang, L. S. (2003) *FEBS Lett* **555**, 13-20
62. Saraste, M. (1984) *FEBS Lett* **166**, 367-372
63. Widger, W. R., Cramer, W. A., Herrmann, R. G., and Trebst, A. (1984) *Proc Natl Acad Sci U S A* **81**, 674-678
64. Crofts, A., Robinson, H., Andrews, K., van Doren, S., and Berry, E. (1988) in *Cytochrome Systems*, (Papa, S., ed), pp. 617-624., Plenum Press, N.Y.
65. Berry, E. A., Zhang, Z., Huang, L. S., and Kim, S. H. (1999) *Biochem. Soc. Transactions* **27**, 565-572
66. Gao, X., Wen, X., Esser, L., Quinn, B., Yu, L., Yu, C. A., and Xia, D. (2003) *Biochemistry* **42**, 9067-9080
67. Gray, K. A., Dutton, P. L., and Daldal, F. (1994) *Biochemistry* **33**, 723-733
68. Xu, J. X., Xiao, Y., Wang, Y. H., Li, X., and Gu, L. Q. (1993) *Biochim Biophys Acta* **1142**, 83-87
69. Berry, E. A., Huang, L.-S., Saechao, L. K., Pon, N. G., Valkova-Valchanova, M., and Daldal, F. (2004) *Photosynthesis Research* **81**, 251-275
70. Kim, H., Xia, D., Yu, C. A., Xia, J. Z., Kachurin, A. M., Zhang, L., Yu, L., and Deisenhofer, J. (1998) *Proc Natl Acad Sci U S A* **95**, 8026-8033
71. Enders, D., Geibel, G., and Osborne, S. (2000) *Chemistry* **6**, 1302-1309
72. Palsdottir, H., Lojero, C. G., Trumpower, B. L., and Hunte, C. (2003) *J Biol Chem* **278**, 31303-31311
73. Berry, E. A., Huang, L. S., Zhang, Z., and Kim, S. H. (1999) *J Bioenerg Biomembr* **31**, 177-190
74. Gao, X., Wen, X., Yu, C., Esser, L., Tsao, S., Quinn, B., Zhang, L., Yu, L., and Xia, D. (2002) *Biochemistry* **41**, 11692-11702

75. Schnauffer, A., Sbicego, S., and Blum, B. (2000) *Curr Genet* **37**, 234-241
76. Manion, M. K., O'Neill, J. W., Giedt, C. D., Kim, K. M., Zhang, K. Y., and Hockenbery, D. M. (2004) *J Biol Chem* **279**, 2159-2165
77. Lovell, S. C., Word, J. M., Richardson, J. S., and Richardson, D. C. (2000) *Proteins* **40**, 389-408
78. Berry, E. A., Guergova-Kuras, M., Huang, L. S., and Crofts, A. R. (2000) *Annu Rev Biochem* **69**, 1005-1075
79. Kabsch, W., and Sander, C. (1983) *BIOPOLYMERS* **22**, 2577-2637

FOOTNOTES

*We would like to thank Antony R. Crofts, Patrick Crowley, Fevzi Daldal, Chris Earnshaw, Hideto Miyoshi, Graham Sexton, Bernard L Trumpower, and Ya-Jun Zheng for helpful discussions during the course of this work and/or reading the manuscript and providing valuable suggestions. This work was supported by NIH research grants DK44842 from NIDDK and by GM62563 from NIGMS. Lawrence Berkeley National Lab (LBNL) is operated by the Department of Energy, contract DE-AC03-76SF00098 to the University of California. Diffraction data were collected at the Advanced Light Source (ALS) at LBNL and at the Stanford Synchrotron Radiation Laboratory (SSRL), which is operated by the Department of Energy, Office of Basic Energy Sciences. The SSRL Biotechnology Program is supported by the National Institutes of Health, National Center for Research Resources, Biomedical Technology Program, and by the Department of Energy, Office of Biological and Environmental Research. We would like to thank Henry Belamy, Nick Sauter, Aina Cohen, and Dan Harrington at SSRL, and Keith Henderson and Corie Ralston at the ALS, for help with data collection; and Nick Sauter at LBNL for advice on data processing. The PDB entries 1PP9 and 1PPJ were processed by Shri Jain and Rose Oughtred of RCSB. The crystals leading to structures 1PP9 and Y21 were grown by Mr. Yusef Collins, at that time supported by a supplement to NIH grant GM62563.

¹Recent evidence suggests that antimycin may play an unrelated role in apoptosis, binding to the anti-apoptotic factor BCL-X_L and inhibiting its suppression of apoptosis (76).

²Abbreviations used are: antimycin, antimycin A; cyt *bc*₁, cytochrome *bc*₁ complex; DM, dodecyl maltoside; HG, β-hexyl-D-glucopyranoside; FSA, formylaminosalicylate moiety of antimycin; CC correlation coefficient; PDB, Protein Data Bank; IUCr, International Union of Crystallographers; NIH National Institutes of Health; URL, uniform resource locator; 2F_o-F_c map, a map from Fourier coefficients calculated as twice the measured amplitude minus amplitude calculated from the structure, and phases calculated from the structure. "N-side" and "P-side" refer to the normally negative matrix side and positive inter-membrane side of the inner mitochondrial membrane. Structures that have been deposited in the PDB are referred to by their capitalized 4-character accession codes (e.g. "1P84"). Their authors and literature references can be obtained from the entry at the PDB if not given here.

³Stereo figures are designed for divergent or "wall-eyed" viewing. An alternate set of figures for "cross-eyed" viewing is available in pdf format in the supplemental materials related to this paper.

⁴Rotamer numbers used here refer to the lists of rotamers provided with the molecular visualization/modeling program O (48), with the most frequently-occurring being in each

case rotamer 1. Lysine rotamer 26 is an exception, coming from the more extensive collection of rotamers in reference (77). The actual side-chain dihedrals of the rotamers referred to are listed in Table S1 (supplemental materials).

⁵Figure 5 is a subset of seven stereo diagrams showing the makeup of the antimycin binding site. The full set is available in pdf format in the supplemental materials related to this paper, and can be referred to to further clarify the relationship of these residues and atoms.

⁶There are different conventions for naming the atoms in antimycin, so we have tried to specify atoms from a chemical standpoint rather than by name. The protein database maintains two versions of antimycin, AMY (from 3BCC) and ANY (introduced with 1PPJ). These have the same atom names, but in ANY two additional carbon atoms have been added to the end of the acyl chain to allow for the possibility that it is heptyl, and the methyl group on the acyl chain has been moved from the 3- to 2- position in accordance with the results of (40). In the Cambridge Structure Database of small molecule structures there is (CCDC # 125007) from the work of Deisenhofer's group (40), which uses different atom names. The PDB entry 1NTK uses the atom names from the Cambridge Database but the residue name (AMY) from the Protein Data Bank. The atom names here, where used in the text and in Table 3, are from ANY of 1PPJ.

⁷The pyrrole rings of heme referred to here as A, B, C, and D correspond to protoporphyrin rings conventionally labeled IV, I, II, and III.

⁸Secondary structure nomenclature for subunits 1 and 2 is defined in Figure 5 of (ref. 44).

Fig. 1. The structure of antimycin (stereo views³). **A**, From the small-molecule crystal structure ((40) ; coordinates form the Cambridge Structure Database, CCDC # 125007). Hydrogen atoms have been removed from the carbon atoms for clarity. **B**, from the structure 1PPJ, with the FSA ring and amide group in the plane of the picture. **C**, as **B** but rotated 75° to view the dilactone ring nearly face-on. The electron density in parts **B** and **C** is a $2F_o - F_c$ map contoured at 2.1 σ (**B**) or 0.9 σ (**C**) from structure 1PPJ.

Fig. 2. Representative density in well-ordered parts of the structure. **(a)**. Heme-ligand met160, showing chirality about the S δ atom. **(b)**. Stigmatellin **(c)** hexyl glucoside molecule sandwiched in a crystal contact. The maps are $2F_o - F_c$, calculated from data between 15 and 2.1 Å, sharpened with B -20, and contoured at 2.3 σ (**a**), 2.0 σ (**b**), or 1.8 σ (**c**); from structures 1PP9 (**a**) or 1PPJ (**b**), (**c**).

Fig. 3. Secondary structure diagram of mitochondrial cytochrome b. (Modified from references (20,78).) The residue-number assignments are based on analysis of the 1PPJ structure by the program DSSP (79)

Fig. 4. H-bonding around the high potential cyt b heme. **(a)**- Heme **b_H** viewed from helix B. Water W4 bridges between the two heme propionate side chains, while W5 bridges between a propionate and the heme axial ligand His97. Arg100 interacts directly with this "bent" propionate, and via unlabeled water molecule W6 with the carbonyl O of His97. W5 is also H-bonding with backbone atoms of helix A, which has been removed from this view for clarity. **(b)**. - The same region viewed from the heme position, looking toward helices A and B. The heme is removed except the two propionate side chains. Intercolation of waters W3 and W5 in the helical backbone of Helix A can be seen. Waters W1-3 are discussed in the text in connection with antimycin binding. The map is a $2F_o - F_c$ map calculated from data between 15 and 2.1 Å, sharpened with B -20, and contoured at 1.8 σ (**a**) or 1.7 σ (**b**).

Fig. 5. Structure of the Q_i site and interaction with bound antimycin⁵. The Q_i site lies in a triangular volume formed by helices **B** and **E** crossing at an angle **(a)**. The N-side (N-terminal) ends of these helices are held together by β -type H-bonding between residues just preceding the helices (arrows in cartoon) which bounds the third side of the volume, and by Lys228 of helix E which H-bonds with a backbone O of residue 27, and to a water molecule bonded to that atom and to Asn32 O_{yl} of Helix A. These bonds are part of a more extensive H-bonding chain involving also Trp31, Ser35 and two other waters. In **(b)** antimycin (magenta bonds) and heme **b_H** (orange bonds) are added. The methyl and propionate substituents of the "A" ring of heme protrude from the four-helix bundle between helices **A** and **D** (helix **D** removed for clarity), forming part of the surface of the binding site. The formylaminosalicylate headgroup of antimycin inserts into the triangular volume described above, sandwiched between Phe220 of helix E and the heme propionate, and H-bonding with Asp228 and (via another water) Lys227. In **(c)** the protein elements shown in **(a)** are rendered as space-filling model to show the surface of the binding site. Antimycin (magenta carbons) and heme **b_H** (orange carbons) are also space-filled to show the intimate contact between these moieties and the snug fit of the antimycin headgroup in the protein. The binding pocket is completed by the α -a surface helix (shown here starting with residue 15) and the **D** transmembrane helix, left as a ribbon for clarity. There may be H-bonds involving His201 in helix **D** with the amide carbonyl oxygen of antimycin and with a backbone oxygen in the α -a helix.

At the lower extreme of antimycin is the aromatic ring, viewed edge-on and inserted between the bent propionate of heme **b_H** and Phe220 in helix **E**. The carbonyl oxygen of the amide

linkage is directed toward the viewer, seen beneath His201 of helix **D**. Higher up, the alkyl side chain extends to the right into the lipid-filled cleft. At the top is the acyl group, with the ester carbonyl oxygen direct towards the viewer. Note the close contact with heme b_H , involving not only the aromatic ring of antimycin but also part of the dilactone ring.

Fig. 6. Schematic representation of the H-bonded chain involved in antimycin binding. Antimycin and four amino acid side chains of cytochrome b are shown as ball-and-stick figures. Water molecules are small red spheres. H-bonds are indicated by thin red lines. Asn32, Ser35, and water W3 are above the plane of the rest of the figure. W3 has been moved slightly for clarity, it is actually nearly over the phenolic OH of antimycin. A H-bond from Ser35O γ to the Asn32O has been omitted, also for clarity.

Fig. 7. Ser35 carbonyl O faces away from antimycin, and Lys227 interacts with antimycin through a water molecule. (a) Ser35 and vicinity: a $2F_o-F_c$ map contoured at 1.5σ . Asp228 has been removed for clarity, and W2 is not shown. (b) Lys227, Asp228, and vicinity: Antimycin is in the front and lower part of the figure, with its formylamino oxygen at the center. Water W1 bridges between the formylamino oxygen and Lys227N ζ at the top of the figure. W1 also makes H-bonds with O γ 1 of Ser32 (left) and the carbonyl oxygen of C27 (right). Also visible in this figure, two-point H-bonding of Asp228 to antimycin. In the background is Asn32 with H-bonds stabilizing W1 and W2, and a bond from the latter atom to Ser35. The intercolated water W3 is behind antimycin, barely visible through the salicyl ring, with H-bond to Ser35 indicated. The map is the same as in (a).

Fig. 8. His201 and Ser205. The view is nearly the same as Figure 7b, showing antimycin, Lys227, Asp228 and water 1. Residues behind those have been removed for clarity, and the C-terminus of helix **D** containing His201 and Ser205 is shown. Two different density levels are used to elucidate the interaction of His201 with antimycin and the possible involvement of a water molecule. The maps are $2F_o-F_c$, contoured at 1.5 in (a) and 1.0 in (b). Also shown is an unknown molecule modeled as dioxygen (see text).

Fig. 9. Flexibility in cyt b induced by antimycin and/or crystal packing forces. Various cyt b structures were aligned based on the relatively rigid core consisting of residues 32-51, 79-99, 113-145, 161-201, and 263-300. Deviations of C α position are plotted vs residue number for selected pairs of structures. For each pair the differences in chain C are shown in red while those for chain P are in blue. The green rectangles along the x axis indicate the position of helices in the sequence. PDB entries 1PP9 (without) and 1PPJ (with antimycin) are the structures featured in this article, while unsubmitted structure Y21 is from a crystal with cell parameters nearly identical to those of 1PPJ. Thus comparison of cyt b from the same monomer between 1PPJ with Y21 (b) gives the best indication of antimycin-induced changes, while comparison of two monomers in the same crystal, or of 1PP9 with Y21 (c), should show only crystal-packing-induced changes. Comparison of 1PP9 with 1PPJ (a) superimposes both sets of changes.

Table 1. Statistics from the structure determination process.

Protein Database entry:	1PP9	1PPJ
Inhibitors co-crystallized:	stigmatellin	stigmatellin, antimycin
A. DATA REDUCTION		
Unit Cell Dimensions	139.12 × 171.06 × 227.20 Å	128.53 × 168.75 × 231.53 Å
Solvent content	58.2 %	54.7 %
V _M	2.97	2.74
X-ray wavelength ¹ :	0.99200	0.97977, 1.0000, 1.1000, 1.1808
Unique Reflections	312369	285923
Resolution Range, Å ¹ :	50 - 2.1 (2.18 - 2.10)	250. - 2.100 (2.15 - 2.10)
"Optical Resolution" ²	1.72 Å	1.75 Å
Completeness:	97.2% (83%)	98.1% (94.3 %)
Data Redundancy:	5.9	5.630
R Merge on I:	0.12 (>1.0)	0.149 (0.879)
<I/σ _I >	10.9 (1.037)	18.6890 (2.819)
B. REFINEMENT:		
Resolution	24.99 - 2.10 (2.15-2.10)	93.53 - 2.10 (2.15 - 2.10)
Data Cutoff (σ _F)	0.0	0.0
Completeness	97.3 (91.9)	97.7% (90.3%)
# Reflections	305496 (19066)	285060 (16565)
R Value	0.250 (0.40)	0.224 (0.33)
Free R Value	0.287 (0.40)	0.260 (0.38)
Number Of Atoms Used		
Protein Atoms	31493	31181
Heterogen Atoms	1005	962
Solvent Atoms	1461	1406
B Values		
From Wilson Plot	27.3 Å ²	33.50 Å ²
Mean atomic B Value	46.9 Å ²	50.20 Å ²
Anisotropic B11, B22, B33	15.35, -0.55, -14.81 Å ²	12.34, -3.71, -8.63 Å ²
ESD,- (cross-validated)		
From Luzzati Plot	0.32 Å (0.39 Å)	0.28 Å (0.35 Å)
From Sigmaa	0.43 Å (0.47 Å)	0.33 Å (0.38 Å)
Rms Deviations From Ideality		
Bond Lengths	0.007 Å	0.006 Å
Bond Angles	1.5°	1.4°
Dihedral Angles	21.8°	21.8°
Improper Angles	1.02°	0.94°
C. VALIDATION:		
Residues in "Most Favored" region of Ramachandran	92.1%	92.4%
Residues in Ramachandran "disallowed" region	0.2%	0.2%
Bad Contacts/100 residues	0.5	0.3
Overall G-factor (ProCheck):	0.4	0.4
Real-space R-value	0.155	0.148
Real-space Correlation Coeff.	0.909	0.921

1. Statistics in the highest resolution shell are given in parentheses.

2. Optical resolution is defined in reference ()

3. Values in parenthesis refer to last shell (resolution) or cross-validated values (ESD).

Table 2. Model completeness by subunit. For each subunit is given the actual number of residues present in the complex based on sequence, and the number of residues modeled in each monomer of the two structures presented here. The chain letters assigned to each subunit in each monomer are also indicated. Major differences are due to the lack of subunit 11 in the crystals and disorder of the first 30 residues of subunit 10 in chain J of 1PPJ.

Subunit	number of residues	modeled in structure:			
		1PP9		1PPJ	
	actual	mono-mer #1	mono-mer #2	mono-mer #1	mono-mer #2
1 "core"1	446	A 442	N 442	A 441	N 441
2 "core"2	439	B 423	O 424	B 424	O 423
3 cyt b	379	C 365	P 370	C 365	P 365
4 cyt c₁	241	D 241	Q 241	D 241	Q 241
5 ISP	196	E 196	R 196	E 196	R 196
6	110	F 99	S 99	F 99	S 99
7	81	G 73	T 74	G 73	T 74
8 "hinge"	78	H 66	U 66	H 66	U 66
9 signal	78	I 42	V 42	I 43	V 43
10	62	J 62	W 62	J 32	W 61
11	56	K 0	X 0	K 0	X 0
sum	2166	2009	2016	1980	2009

Table 3. Residues surrounding Antimycin at the Q₁ site. For each contact closer than 4 Å is given the residue type, number, and atom; the atom of antimycin, and the contact distance in each monomer. For distances greater than 3 Å, only the closest contact of each protein residue is given. Except for waters, all the residues contacting antimycin belong to cyt b (chains C and P). The "water" modeled between His201 and antimycin O3 does not account for the density as currently modeled (Figure 8).

Helix A and Waters (W)				Helix D & E				Heme bH			
protein atom	Anti atom	distance (Å)		protein atom	Anti atom	distance (Å)		Heme atom	Anti atom	distance (Å)	
		C	P			C	P			C	P
ALA17	O C10	3.6	3.7					HEM502	CMA N2	3.8	3.8
ILE27	CD1 O2	3.5	3.5	MET190	CG C23	4.0	3.7	HEM502	CMA C9	3.8	3.7
TRP31	O N1	3.4	3.4	MET194	CG O9	3.6	3.5	HEM502	CMA O4	3.2	3.2
ASN32	OD1 C8	3.9	3.9	LEU197	CD1 O4	3.2	3.1	HEM502	CMA C20	3.3	3.3
GLY34	O C27	3.9	4.0	SER205	OG C4	3.5	3.5	HEM502	CMA O7	3.7	3.7
SER35	CA O7	3.0	3.1					HEM502	CMA C27	3.9	3.9
GLY38	CA C27	3.8	3.8	PHE220	CE1 C1	3.3	3.4	HEM502	CAA C5	3.8	3.9
LEU41	CD2 C25	3.9	3.7	TYR224	CD1 O2	3.3	3.3	HEM502	CAA C6	3.8	3.9
				ASP228	OD1**N1	2.8	2.8	HEM502	CAA C7	3.9	4.0
W3	O ** O1	2.9	2.8	ASP228	OD2**O1	2.6	2.6	HEM502	CBA C1	3.8	3.8
W1	O ** O2	2.6	2.6					HEM502	CBA C5	3.7	3.8
"W"	O O3	2.6	2.8					HEM502	CBA C6	3.6	3.6
W1203	O C5	---	3.7								

Table 4. Potential H-bonding partners for six highly-ordered water molecules in the region of heme b_H and the Q_i site. For each of the waters, O and N atoms within 3.5 Å are listed, together with the interatomic distance in each of the two monomers (chains C and P). The B-values for the waters in each monomer are also given.

Label	Water res.		H-bond Partner			Distance		B-value	
	(C,	P)	Res.	Num	Atom	C	P	C	P
W4	168	109	** SER	205	OG	2.5	2.5	27	31
			** HEM	502	O2A	2.8	2.8		
			** HEM	502	O1D	2.7	2.7		
W5	2	1	** HEM	502	O1A	2.5	2.6	33	30
			** TRP	30	O	2.8	2.7		
			** HIS	97	ND1	2.9	2.8		
			** PHE	33	N	3.1	3.3		
			** GLY	34	N	3.1	3.4		
			ARG	100	NH1	3.5	3.4		
ARG	100	NH2	3.5	3.2					
W6	108	35	** HIS	97	O	2.6	2.7	31	32
			** ARG	100	NE	3.2	3.1		
			** ARG	100	NH2	3.2	3.0		
			** GLY	101	N	3.3	3.4		
W1	119	959	** Antimycin		O2	2.6	2.6	44	38
			** LYS	227	NZ	2.6	2.6		
			** SER	28	O	3.1	2.9		
			** ASN	32	OD1	3.2	3.3		
W2	1008	214	** SER	35	OG	2.7	3.0	29	32
			** ASN	32	ND2	2.8	2.8		
			** ASP	228	O	3.0	2.7		
W3	222	28	Antimycin		N1	3.2	3.2	25	32
			** Antimycin		O1	2.9	2.8		
			** TRP	31	O	2.7	2.7		
			ASN	32	O	3.2	3.2		
			** SER	35	N	2.8	2.8		
** SER	35	OG	3.0	2.9					

** - potential hydrogen bond

Table 5. Relative motion of domains of cyt. b between three crystals:F₂,G,H helices vs cyt. b core

	-----Chain C-----			-----Chain P-----		
	angle	max disp,	atom	angle	max disp,	atom
1PP9 vs 1PPJ	1.392	0.8389	C378	1.169	0.6904	P378
1PPJ vs Y21	0.437	0.3072	C378	0.310	0.2654	P377
1PP9 vs Y21	0.960	0.5969	C378	0.944	0.5979	P378

E helix after 227 vs cyt. b core

	-----Chain C-----			-----Chain P-----		
	angle	max disp,	atom	angle	max disp,	atom
1PP9 vs 1PPJ	0.927	0.3315	C245	0.503	0.1145	P245
1PPJ vs Y21	0.301	0.1486	C245	0.513	0.1814	P230
1PP9 vs Y21	0.859	0.2438	C245	0.349	0.1600	P228

Table 6. Residues surrounding stigmatellin at the Q_o site. For each residue is given the residue chain, type and number; the closest atom in the residue to stigmatellin, the closest atom of stigmatellin, and the distance between these two atoms. The residues are divided into the three areas discussed in the text.

Headgroup pocket:				Hydrophobic orifice:				Outside surface:			
protein	Stig.	dist-		protein	Stig.	dist-		protein	Stig.	dist-	
residue	atom	atom	ance (Å)	residue	atom	atom	ance (Å)	residue	atom	atom	ance (Å)
R:HIS161	NE2**O4		2.80	C:PHE274	CD1	C22	3.51	C:ALA125	N	O14	3.78
R:HIS161	NE2	O5	3.30	C:MET124	CB	O14	3.83	C:ILE146	CG2	C15	3.71
R:CYS160	CB	C5M	3.60	C:ILE146	CD1	C10	4.54	C:LEU121	O	C25	3.46
C:GLU271	OE1**O8		2.54	C:ILE298	CG1	C23	4.09	C:PHE178	CE1	C21	4.00
HOH299	O	**O8	2.80	C:ALA277	CB	C22	3.82	C:MET129	CE	C21	3.68
C:TYR278	CD1--O4		3.12	C:LEU294	CD2	O12	3.85	C:ILE164	CG2	C21	4.03
C:PRO270	CB	C8	3.55	C:LEU149	CD1	O12	4.69	C:PHE181	CD2	C21	4.21
C:VAL145	CG1	O5	3.46	C:PHE128	CE2	C18	3.82	C:THR147	OG1	C26	4.07
C:MET138	O	C7M	3.47					C:LEU150	CD1	C26	4.55
C:TRP141	C	C7M	4.51								
C:ILE268	CD1	C7M	3.99								
C:GLY142	CA	O7	3.64								
C:ILE146	CD1	O1	3.56								
C:LEU281	CB	C3M	4.50								

**Hydrogen bond

--Putative unconventional hydrogen bond (72).

Appendix. List of supplementary materials available with this article.

1. Procheck validation reports for structures 1PP9 and 1PPJ

1pp9-procheck.pdf, 1ppj-procheck.pdf

2. sfcheck validation reports for structures 1PP9 and 1PPJ

1pp9-sfcheck.pdf, 1ppj-sfcheck.pdf

3. Set of figures with stereo for cross-eyed viewing: **Figuresx.pdf**

4. Expanded Figure 5 with 7 views, one per page:

antipocket.pdf, (antipocketx.pdf for cross-eyed viewing).

5. Other.pdf:

Scheme S1. Q-cycle mechanism

Figure S1. Stereodiagram, space-filling model of cyt b helix A backbone with intercolated waters W3 and W5.

Figure S2. Stereo views of omit map density for antimycin in 1PPJ.

Figure S3 - S7. Stereo views of omit map density for critical residues in 1PPJ

S3. C:Ser35

S4. C:Lys227

S5. C:His221-Pro222 cis-peptide

S6. C:His345-Pro346 cis-peptide

S7. D:Gly73-Pro74 cis-peptide

Table S1. List of standard rotamers referred to, defined by side-chain dihedral angles:

6. **VRML views** of the structure with electron density to allow examination from any angle.

These can be viewed in a web browser equipped with a VRML plugin or helper application such as:

For Windows: Cosmo-viewer or Cortona (www.parallelgraphics.com/products/cortona).

For Linux: FreeWRL or vrmlview (<http://www.sim.no/download/>).

For Irix: Cosmoviewer (available for download from the Silico Graphics website).

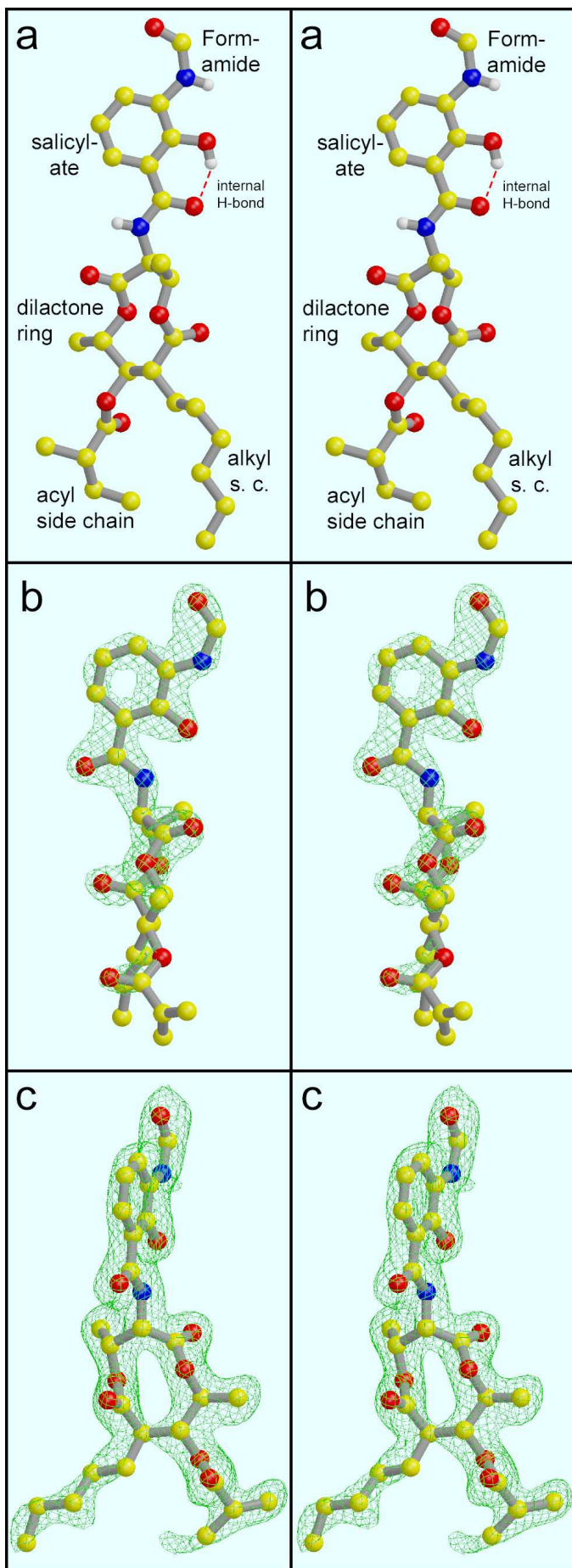


Figure 1
Huang et al.

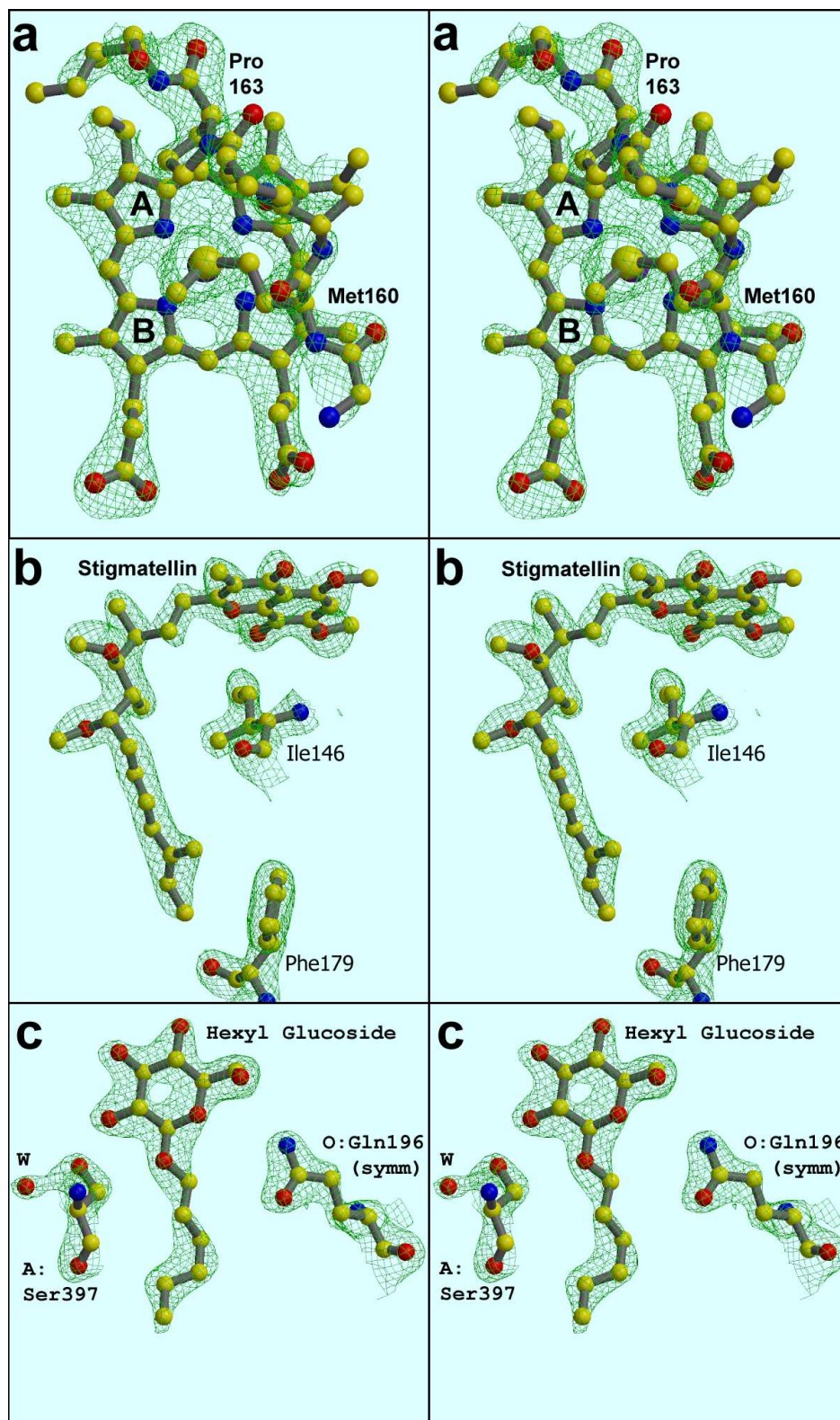


Figure 2
Huang et al.

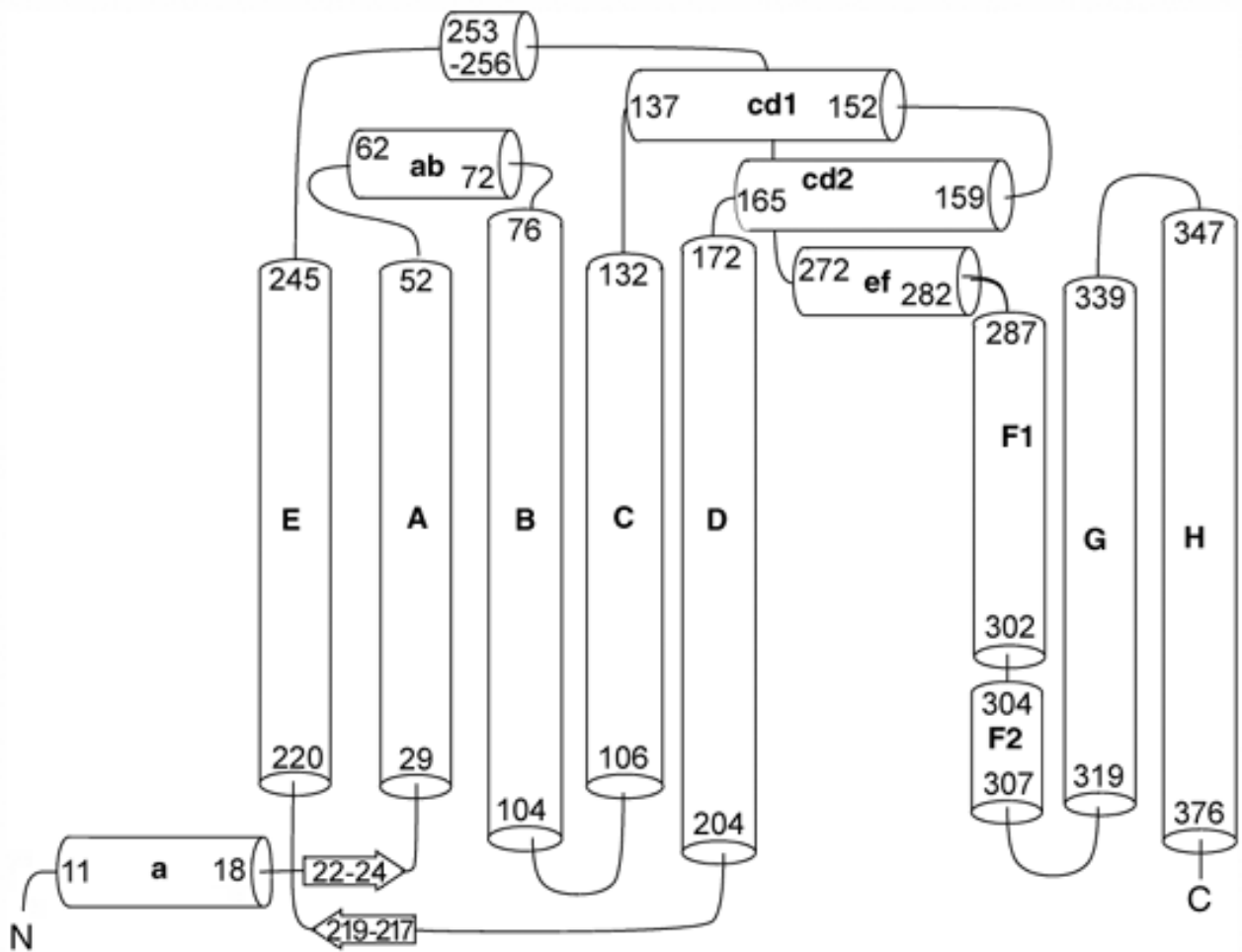


Figure 3
Huang et al.

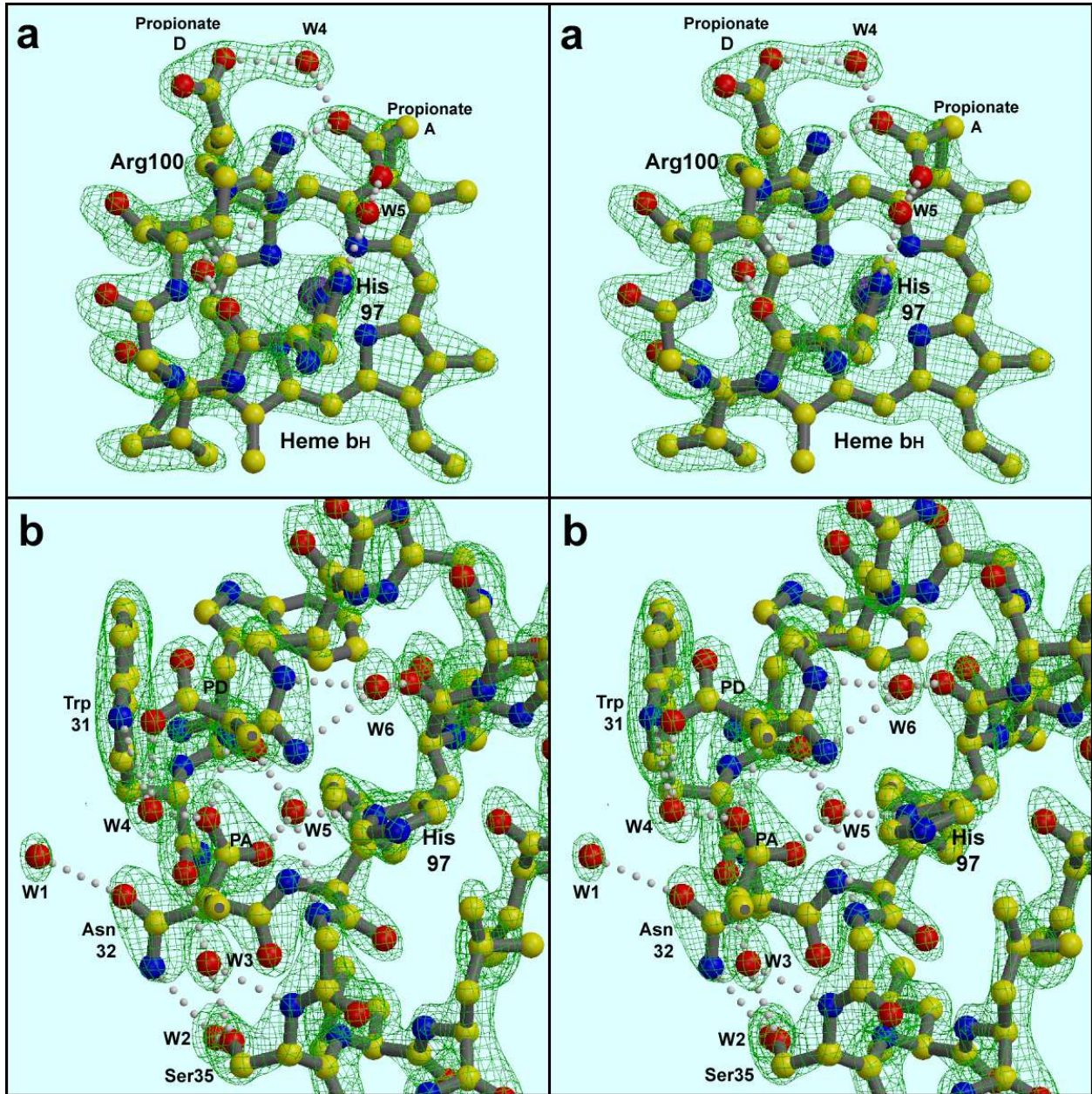


Figure 4
Huang et al.

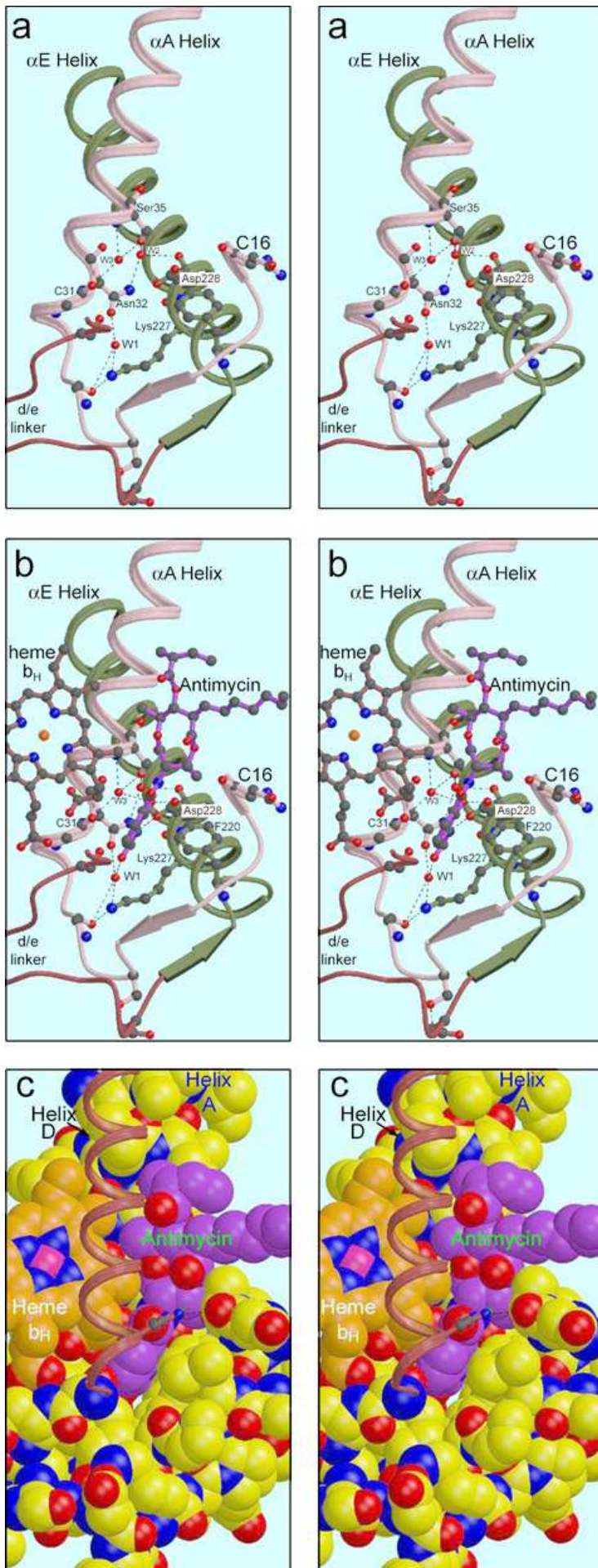


Figure 5.
Huang et al.

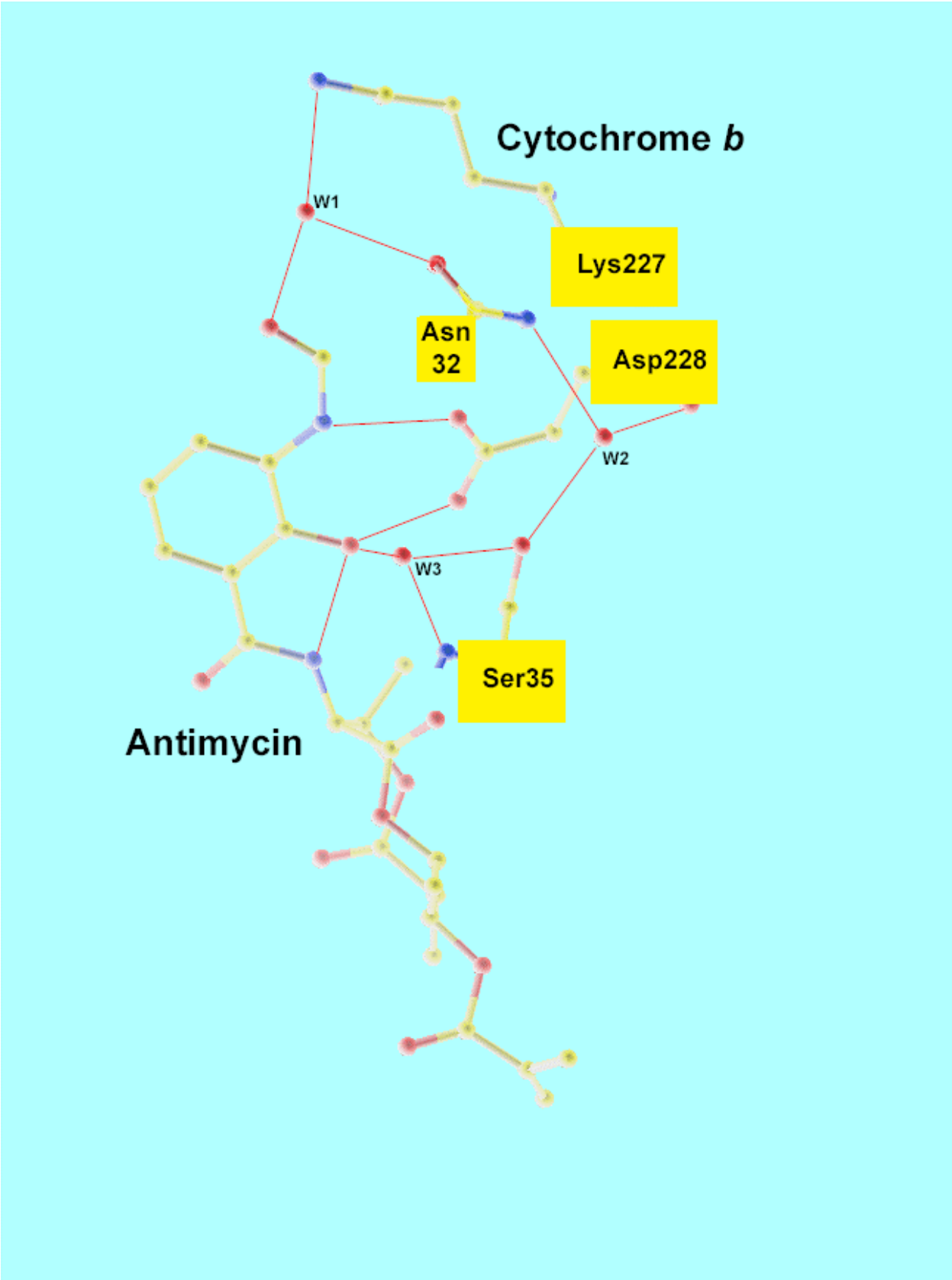


Figure 6
Huang et al.

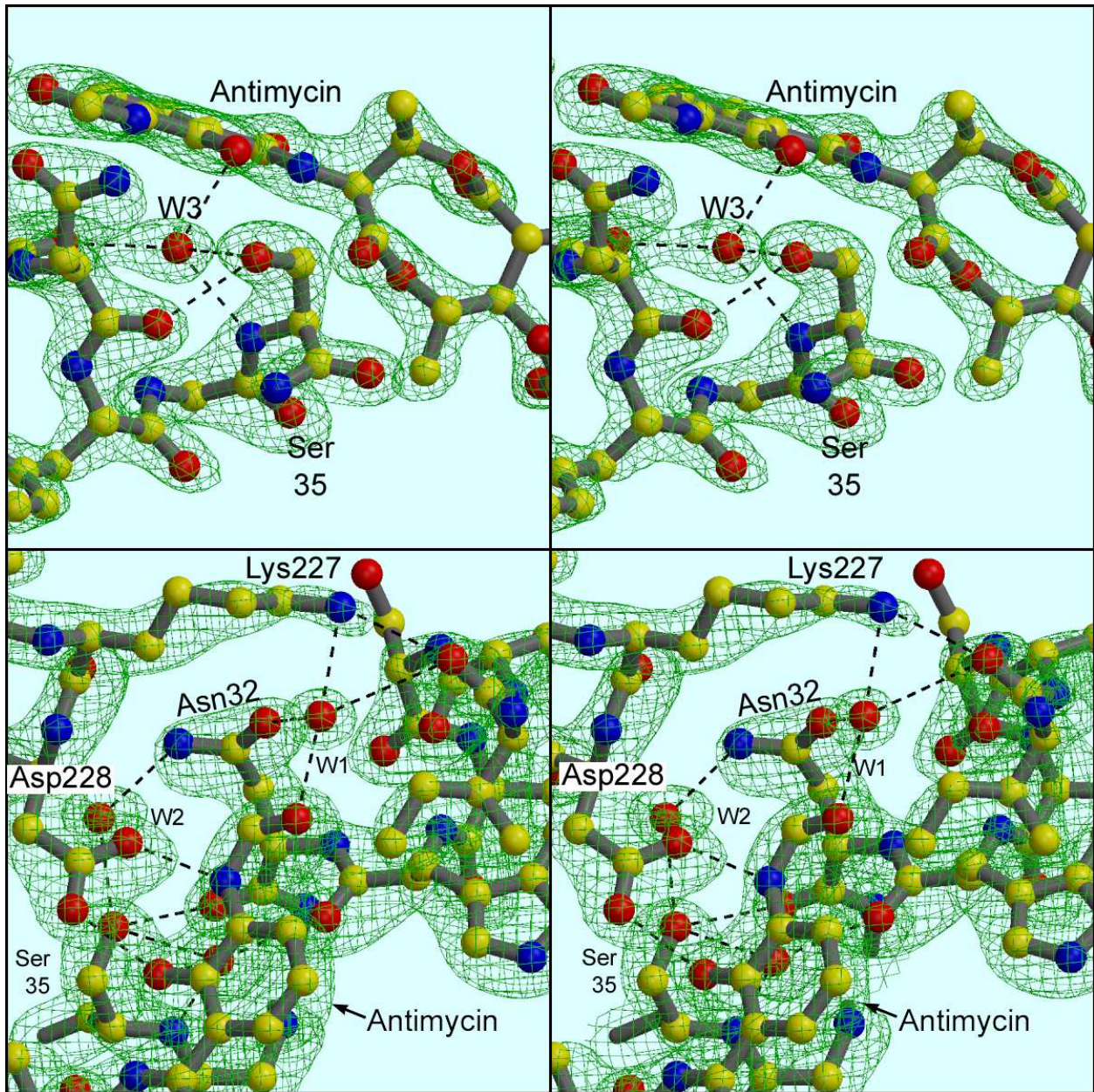


Figure 7
Huang et al.

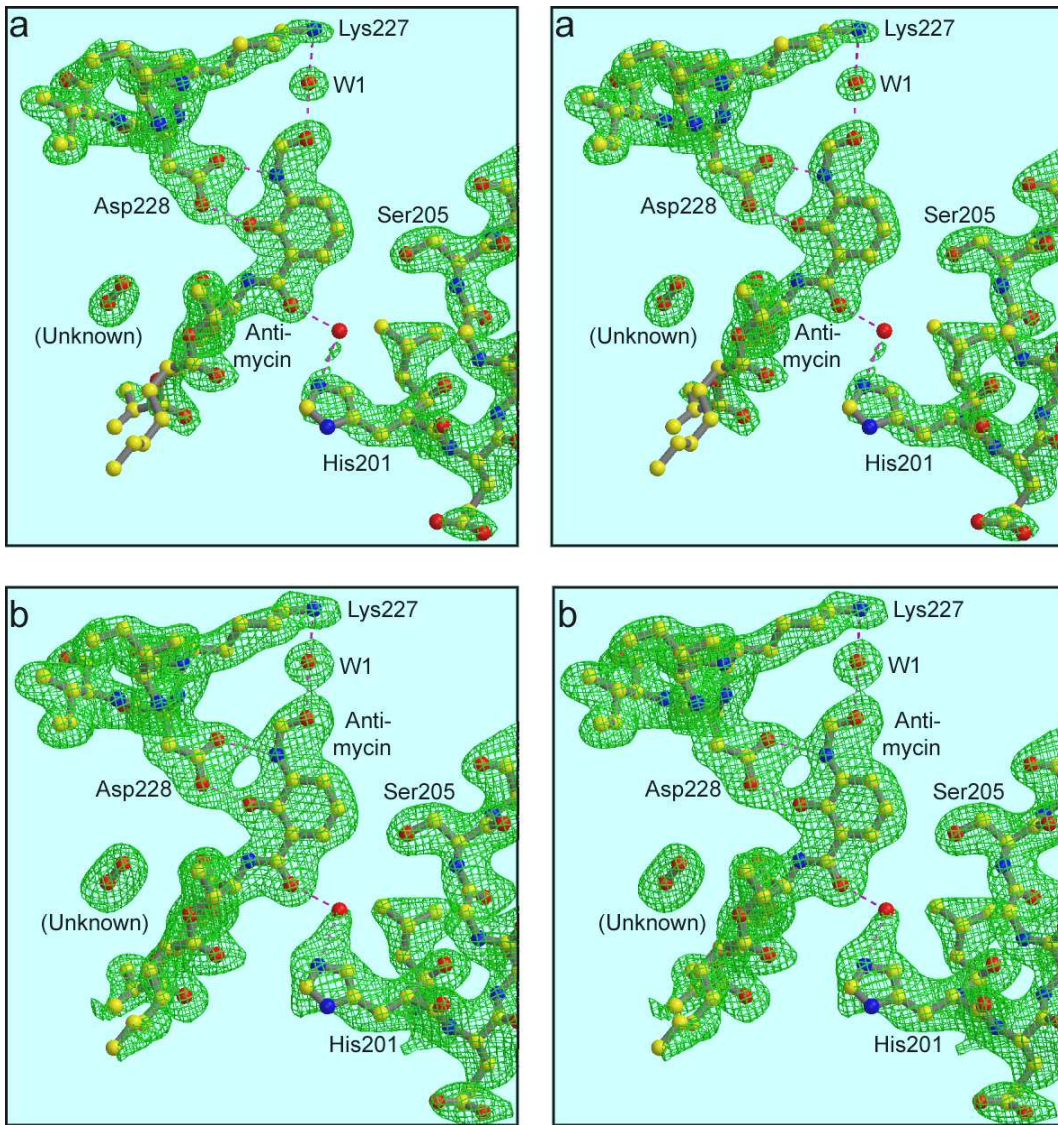


Figure 8
Huang et al.

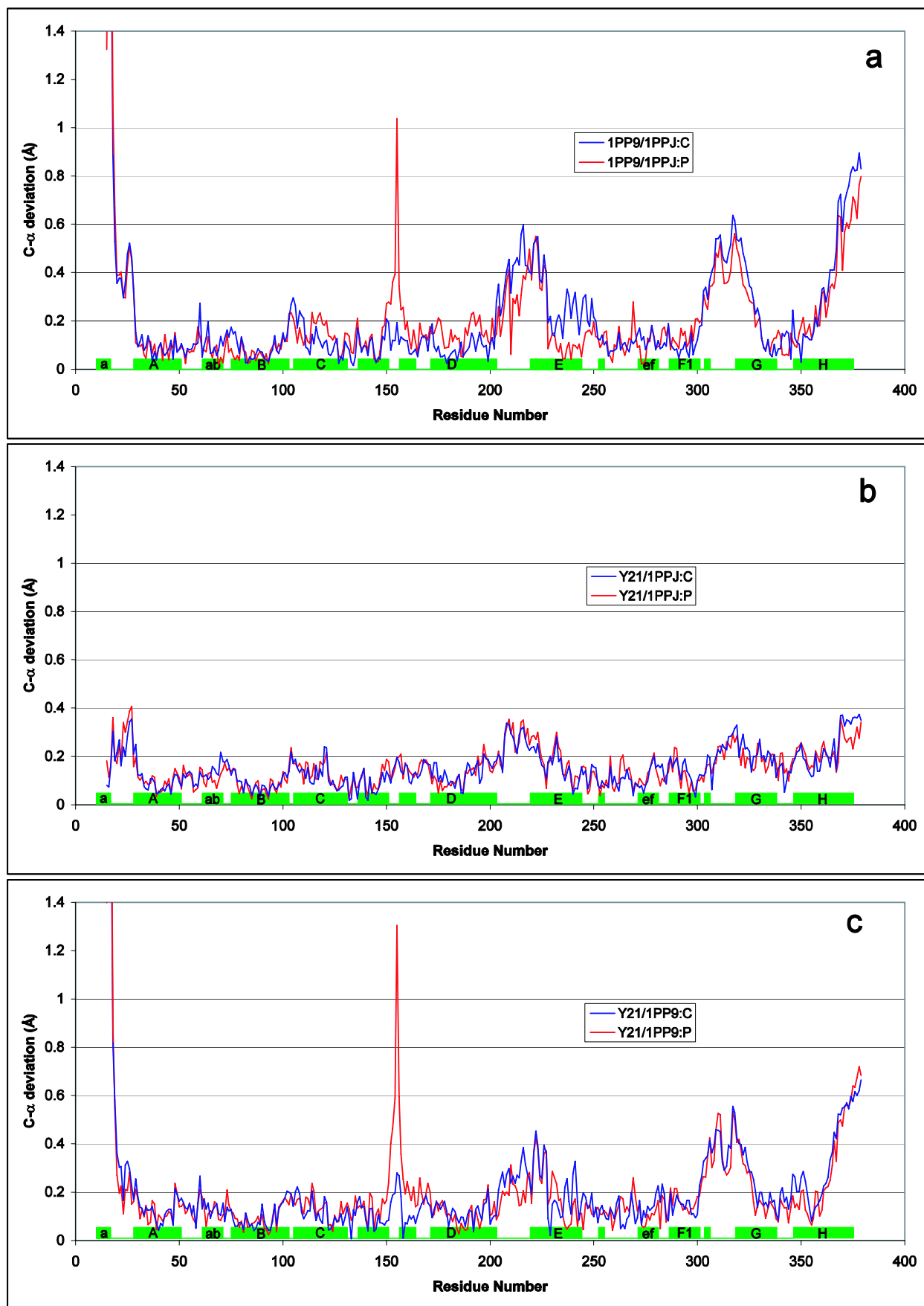


Figure 9
Huang et al.